Space Science Reviews (2025) 222:1
https://doi.org/10.1007/s11214-025-01251-w

The Compact Dual Ion Composition Experiment (CoDICE) for the IMAP Mission

S.A. Livi[1,2] · M.I. Desai[1,2] · K. Ogasawara[1,2] · L. Kistler[3] · E. Möbius[3] · M.J. Starkey[1] · M.A. Dayeh[1,2] · D. Kataria[1] · H.A. Elliott[1,2] · S. Hart[1] · B. Alterman[4] · D.J. McComas[5] · C.J. Pollock[4] · J. Mukherjee[1] · J. Trevino[1] · S. Ferrell[1] · T. Brenner[1] · S.E. Pope[1] · M. Tapley[1] · K. Pavlas[1] · J.S. Rankin[5] · M.M. Shen[5] · L. Khoo[5] · M. Alimaganbetov[5] · J. Teifert[5] · E.M. Roemer[5] · M. Shaw-Lecerf[5] · J. Escobar[5] · E.R. Christian[4] · N.A. Schwadron[3,5] · M. Gkioulidou[6] · G. Grubbs[1] · M. Brysch[1] · M. Epperly[1] · D. George[1] · G. Dunn[1] · J. Ford[1] · C.L. Schwendeman[1] · M. Commons[7] · S. Persyn[1] · S. Jaskulek[6] · S. Weidner[5] · C. Bert[1] · M. Ferris[1] · B. Rodriguez[1] · C. Nunez[1] · C. Urdiales[1] · S. Cortinas[1] · H. Rodriguez[1]

Received: 18 September 2025 / Accepted: 23 November 2025 / Published online: 16 December 2025

Abstract
Stationed in an orbit about the first Sun-Earth Lagrange point, L1, NASA's Interstellar Mapping and Acceleration Probe (IMAP) mission is designed to provide well-coordinated measurements of the in-situ solar wind (SW) plasma and interplanetary magnetic field, interstellar pickup ions (PUIs), suprathermal and energetic ions, interstellar and energetic neutral atoms (ENAs), interstellar dust, and 3-dimensional (3D) maps of the global solar wind structure. Together these measurements from ten instruments address two key Heliophysics objectives, namely, 1) the acceleration of charged particles and 2) the interaction of the solar wind with the local interstellar medium. This paper describes one of the five in-situ instruments – the Compact Dual Ion Composition Experiment (CoDICE) that provides comprehensive measurements of the source populations and the charged particles that are accelerated near the Sun and throughout the heliosphere and beyond. CoDICE also provides the 3D velocity distribution functions (3D VDFs) of interstellar PU He^{+} ions and the isotopic composition of interstellar He and Ne PUIs, thus enabling detailed studies of the properties of the local interstellar medium (LISM) and its interactions with the SW and our heliosphere. CoDICE is a next generation instrument that combines two measurement systems in a novel, compact design to provide 1) the 3D VDFs and mass, isotopic, and ionic charge state composition of the lower energy SW, suprathermal, and PUIs between ∼0.5–80 keV/q, and 2) the arrival directions, and mass and isotopic composition of higher energy H-Fe ions between ∼0.03–5 MeV/nuc. CoDICE also provides measurements of SW abundances and charge states, as well as the intensities of suprathermal protons in four different directions to the real-time I-ALiRT data stream for Space Weather research and monitoring.

Keywords Sun · Heliosphere · Particle acceleration · Suprathermal ions · Energetic particles · Solar wind plasma · Pickup ions · Space weather · IMAP

Extended author information available on the last page of the article

1 Introduction

The Interstellar Mapping and Acceleration Probe (IMAP) is the fifth mission in NASA's Heliophysics Solar Terrestrial Probe (STP-5) program whose goal is "to understand the physical processes that determine the mass, momentum, and energy flow in the solar system from the Sun to planetary bodies including Earth, and to understand the interstellar boundary and its interaction with the local interstellar medium."

The IMAP mission's four science objectives are (McComas et al. 2025)

1) *Improve understanding of the composition and properties of the local interstellar medium.*
2) *Advance understanding of the temporal and spatial evolution of the boundary region in which the solar wind and the interstellar medium interact.*
3) *Identify and advance understanding of processes related to the interactions of the magnetic field of the Sun and the local interstellar medium.*
4) *Identify and advance understanding of particle injection and acceleration processes near the Sun, in the heliosphere and heliosheath.*

To achieve these objectives, IMAP determines the properties of the local interstellar medium and the acceleration of suprathermal populations, resolved in angle and energy, over the spectral range to cover all key particle populations using a comprehensive suite of 10 instruments on board a simple sun-pointed spinner stationed in a halo orbit around the Sun-Earth L1 Lagrangian point. In this paper we describe the Compact Dual Ion Composition Experiment (CoDICE; see Desai et al. 2015, 2016, 2017) which is one of five in-situ instruments that together address objectives 3 and 4 through measurements of charged particles that are accelerated near the Sun and throughout the heliosphere and beyond (Cohen et al. 2026). The five in-situ instruments complement each other by providing comprehensive measurements of the distribution, composition, and energy spectra of the solar wind, suprathermal, and energetic ions (protons through Fe) and electrons from <100 eV to above 40 MeV/nuc (see Rankin et al. 2025; Horbury et al. 2026; Christian et al. 2026; Skoug et al. 2026). CoDICE also addresses Objective 1 by providing 3-Dimensional (3D) velocity distribution functions (3D VDFs) of interstellar pickup He^+ ions and the isotopic composition of He^+ and Ne^+ (Szalay et al. 2026). The IMAP mission also incorporates the IMAP Active Link for Real-Time (I-ALiRT) system to provide continuous, near-real-time telemetry essential for operational space-weather monitoring (McComas et al. 2025; Lee et al. 2025). CoDICE provides 1) solar wind (SW) charge-state and elemental abundance ratios (e.g., C^{6+}/C^{5+}, O^{7+}/O^{6+}, Fe/O) at 4-minute cadence, and 2) measurements of $\sim$0.1–3.5 MeV protons in four different directions at $\sim$1 minute cadence to the I-ALiRT data stream.

CoDICE is a next generation instrument that combines two measurement systems in a novel, compact design to measure the 1) elemental, ionic charge state, and isotopic composition and the 3D velocity distribution functions (VDFs) of solar wind He–Fe ions and interstellar pickup He, O, and Ne ions in the $\sim$0.5–80 keV/q energy range in CoDICE-Lo, and 2) the mass composition and arrival direction of $\sim$0.03–5 MeV/nuc ions in CoDICE-Hi (Desai et al. 2015, 2016, 2017). These measurements are required to 1) determine the LISM composition and flow properties, and 2) discover the origin of the enigmatic suprathermal tails and advance understanding of the acceleration of particles in the heliosphere.

Section 2 describes the science objectives, drivers and requirements that flow down from IMAP L1 requirements. Section 3 comprises the high-level sensor description, including operating principles, mechanical, electronics, and thermal designs. Section 4 discusses the sensor SIMION model and simulation results. Section 5 presents results from on-ground

Table 1 CoDICE Science Objectives and Measurement Requirements

Measurement Objective	Mission L2/CoDICE L3 science requirement	
	MRD-L2/ RCODICE-L3	Requirement
Solar wind composition & Charge States for solar wind densities above 3 cm^3 at a cadence: ≤ 1 hour	185/1062	• Composition ratios of C/O, Mg/O, Fe/O with accuracy better than 50% • Charge state ratios of C^{6+}/C^{5+}, O^{7+}/O^{6+}, Fe(low)/Fe(high) with accuracy: better than 50%
Pick-up Ions during nominal slow solar wind conditions	18/1047, 1053	• 3D VDFs of pick-up ions He^+ between 2–18 keV/q in ≥ 5 energy bands per decade • Mass Range and Resolution: H to Ne at M/ΔM > 2 • Angular resolution: ≤15° for He^+ • Isotopic Composition of $^3He^+$, $^4He^+$, $^{20}Ne^+$, and $^{22}Ne^+$ between 2–70 keV/q in ≥ 5 energy bands per decade • Mass range: 3–22 amu • Mass per charge resolution: (M/q)/Δ(M/q) > 10
Suprathermal through Energetic ions	19/1069	• Mass range: H to Fe at M/ΔM > 4 • Energy range: 0.05–2 MeV/nuc at ≥ 5 energy band per decade • Cadence: ≤ 1 min for H; ≤ 10 min for He; ≤ 1hr for O and Fe
Space Weather Broadcast for I-ALiRT	164/1184, 1185	• *Suprathermal Protons:* 1 min. cadence with 4 look directions, 4 spin sectors, an energy range of 0.05–2 MeV, and greater than 5 energy bands (CoDICE-Hi). • *Solar wind charge state and composition ratios*: less than 1 hour cadence, with composition C/O, Mg/O, Fe,O and charge state C^{6+}/C^{5+}, O^{7+}/O^{6+}, Fe(low)/Fe(high) (CoDICE-Lo).

calibration and cross-calibration campaigns. Section 6 describes the engineering and science operational modes and finally, Sect. 7 provides a detailed description of the science data products, including the algorithms used at the SDC and Menlo for processing the raw L0 data into higher-level products.

2 CoDICE Science Objectives & Requirements

CoDICE science measurement objectives can be divided into three broad categories, namely, 1) 3D VDFs and composition of solar wind ions; 2) 3D VDFs and composition of interstellar PUIs; and 3) energy spectra, arrival directions, and mass composition of suprathermal through energetic ions. These objectives flow down from IMAP mission Level 2 requirements to CoDICE Level 3 requirements and are summarized in Table 1.

3 High Level Sensor Description

3.1 Principle of Operation

Figure 1 shows a SIMION model (Dahl 2000) of the CoDICE sensor and Table 2 summarizes key detector systems and performance parameters. The CoDICE sensor comprises two

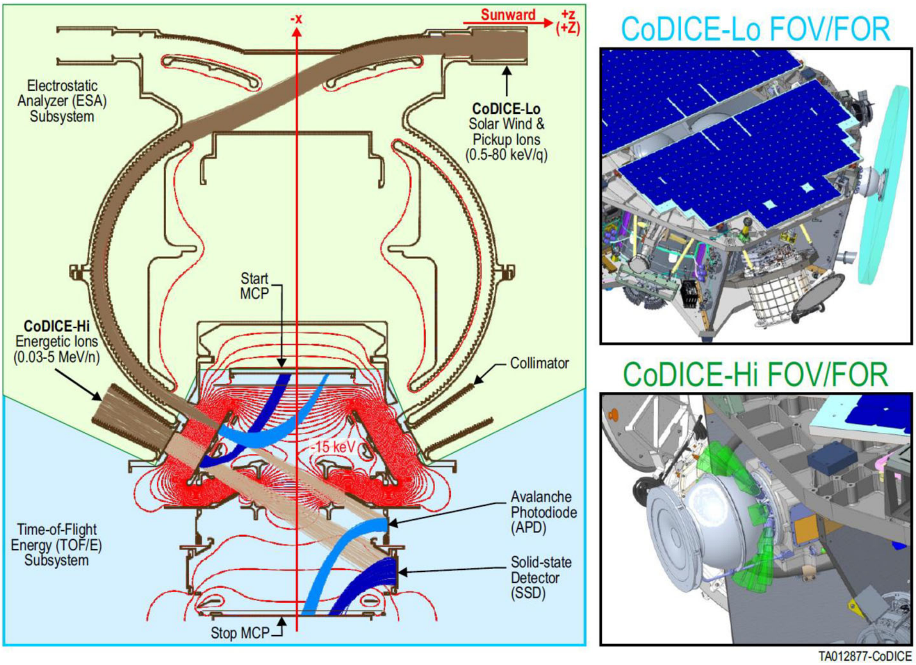

Fig. 1 CoDICE cross-section showing the electro-optical design and SIMION simulations of the primary ion (brown) and secondary electron (blue) trajectories through the ESA and TOF/E subsystems (left). Sample electric equipotential lines in the TOF and ESA subsystems are shown by thin red lines with 600 V increments. Field-of-Views (FOVs) or Field-of-regard (FORs) of the CoDICE-Lo (blue) apertures and the CoDICE-Hi ESA entrance (green). Note -x is in the instrument xyz coordinate system and +Z is in the s/c XYZ coordinate system, defined in Table 2

major sub-systems, namely, 1) an electrostatic analyzer (ESA), and a 2) time-of-flight (TOF) vs. residual energy (E_{Res}) or TOF/E spectrometer. CoDICE-Lo measures ions between ∼0.5 and 80 keV/q that enter the collimated aperture (dark brown trajectories) and are selected according to their E/q and focused by the ESA into the START TOF subassembly. As IMAP rotates at four revolutions per minute (RPM), the full energy range is measured during a 4-minute interval or 16 spacecraft spins by the ESA through 128 voltage steps. The E/q sweeping steps up to the maximum voltage for the next stepping cycle when SW H^+ count rates near ∼1 keV/q exceed a predefined threshold rate. The START subassembly, biased at –15 kV, accelerates the incoming ions before they strike a thin carbon foil (∼0.5–1 $\mu g/cm^2$) at the entrance of the TOF/E subsystem. This interaction produces secondary electrons (light blue trajectories) that are guided to the outer annulus of the START MCP. The azimuthal arrival directions of the incoming ions are determined by a position-sensing delay line embedded within the START MCP subassembly. The mostly neutralized ions (light brown trajectories) then traverse a ∼10.64 cm flight path and strike one of 24 Avalanche Photodiodes (APDs) (Ogasawara et al. 2016) where they generate secondary electrons that are guided to the center of the STOP MCP (light blue). The TOF between the START and STOP MCP signals yields the ion velocity. The E_{Res} of the neutralized ion is measured by one of the 24 azimuthally distributed APDs. The combined measurements, E/q, TOF, and E, determine the mass (M), charge state (q), and M/q.

Table 2 CoDICE Summary & Performance

Item	CoDICE-Lo	CoDICE-Hi
Measurement Objective	Solar wind (SW), Pick-up ions (PUIs), and suprathermal ions	Suprathermal-through-Energetic ions
Instrument type	SW, PUI, suprathermal Ion Mass Spectrometer: Electrostatic Analyzer/Time-of-flight/Residual Energy	Suprathermal & Energetic Ion Mass Spectrometer, Time-of-flight/Residual Energy
Measurement Parameters & Technique	Energy-per-charge (E/q), Time-of-flight (TOF) and Residual Energy (E_{Res})	Time-of-flight (TOF) and Residual Energy (E_{Res})
	• E/q: 128 Electrostatic Analyzer (ESA) Voltage Steps • START TOF & Azimuth (Az): Outer Annulus of START Microchannel plate (MCP) with 24-pixel delay line anode • STOP TOF: Inner circular portion of STOP MCP • TOF pathlength: 10.4 cm • E_{Res}: 24 Avalanche Photodiodes (APDs)	• START TOF: Inner Annulus of START MCP • STOP TOF: Outer Annulus STOP MCP • TOF pathlength: 12.4 cm • E_{Res} & Azimuth (Az): 12 solid-state detectors (SSDs)
Detectors		
Residual Energy	24 APDs, each 300 μm thick, active area 3×5 mm^2	12 SSDs, each 700 μm thick, active area 15×15 mm^2
START Foils	~0.5–1 μg/cm^2 carbon foil at entrance aperture for each of 24 APDs and 12 SSDs	
Collimator Foils	N/A	Two 100 nm foils in each of 12 collimators: One 100 nm Al + One 50 nm Al + 50 nm polyimide
START MCP	68 mm outer diameter, 58 mm Active Area, 1 mm thick	
STOP MCP	86.7 mm outer diameter, 77 mm Active Area, 1 mm thick	
Electronics:		
E/q	7-bit precision for ESA voltage steps	N/A
E_{Res}	9-bit precision with dual gain; threshold~1 keV; High Gain $\lesssim$300 keV; Low gain $\lesssim$1 MeV	11-bit precision with triple gain, threshold ~100 keV; High Gain $\lesssim$5 MeV; Medium gain $\lesssim$35 MeV; Low gain$\lesssim$160 MeV
TOF	10-bit precision; range 0–640 ns	10-bit precision; range 0–160 ns
Az.	5-bit precision from delay line	4-bit precision for SSD location
Spin Sector	5-bit precision from S/C spin pulse	5-bit precision from S/C spin pulse
Species	Interstellar PUIs: PUIs: $^3He^+$, $^4He^+$, N^+, O^+, $^{20}Ne^+$, $^{22}Ne^+$, Ar^+, SW & suprathermals: Mass & Q-states of SW He-Fe	H-Fe
Energy Range & Resolution	0.5–80 keV/q, ΔE/E=4%	Ions: ~0.03–5 MeV/nuc @ 13 bins/decade
Mass Range & Resolution	M: 3–56 amu	M: 1–56 amu
	$(M/q)/\sigma_{(M/q)}$>10–50 (mass dependent)	M/σ_M ~3–10 (mass dependent)
	M/σ_M >2–20 (mass dependent)	

Table 2 (*Continued*)

Item	CoDICE-Lo	CoDICE-Hi
Instantaneous FOV, El. × Az.; Sky Coverage	24 6° × 6.6° apertures over 360° azimuth	12 10°x16° apertures over 360° azimuth
	∼1.8 π sr in full spin	∼2.1 π sr in full spin
Dynamic Range	Quiet time – 10^5 counts/sec	Quiet time – 10^5 counts/sec
Time Resolution	1 hr for 3D VDFs of He^+, <30 min for SW composition	1 min for H, 10 min for He, $\lesssim$1 hr for O and Fe in gradual SEP events
GE of GF	>2.6x10^{-3} cm^2 sr eV/eV; Reduced GF in high SW He^{2+} count rates intervals	∼0.156 cm^2 sr
Observational Modes	E/q scans optimized to reduce H counts and increase duty cycle of suprathermals	None
Mass	16.1 kg	
Volume	44,680 cm^3; Dimensions in instrument coordinate system: x–56.3 cm; y–25.6 cm; z–31.0 cm	
Power	18.5 W @ Hot Operation, 25.1 W average @ Cold Operation	
Raw Telemetry (4-min cycle)	Science: 4762 kbps	Science: 1505 kbps
	I-ALiRT: 115 bps	I-ALiRT: 32 bps

CoDICE-Hi measures ions between ∼0.03–5 MeV/nuc (dark brown in Fig. 1) that enter the common TOF/E subsystem through 12 separate collimators, each with 10°×16° acceptance or FOV in elevation and azimuth. Each collimator has two 100 nm foils (see Sect. 3.2.1) that attenuate UV light to <0.1% and STOP low-energy (<10 keV) protons. START TOF signals are generated by secondary electrons (dark blue) that are produced when the ions pass through the C foils located at the TOF/E entrance and guided to the center of the START MCP. The neutralized ions then traverse a 12.3 cm flight path and strike one of 12 SSDs distributed over 360° azimuth, respectively, where they generate secondary electrons that are guided onto the outer annulus of the STOP MCP. Each SSD, 700 μm thick with an active area of 15×15 mm^2, determines the ion's residual energy E_{Res}. The E_{Res} along with the TOF, which yields the ion velocity, provides the ion mass. The novelty of the CoDICE design is that the START and STOP secondary electrons generated by ions entering both the -Lo and -Hi apertures are detected by the same START and STOP MCPs, respectively but in separate areas.

Figure 2 shows the CoDICE overall block diagram along with the FOVs in the instrument frame xyz coordinate system and the S/C frame XYZ coordinate system. The +z axis in the instrument frame is along the spin axis, +x is along the axis of symmetry of the ESA pointing into the S/C deck (see Figs. 1 and 2), and +y completes the right-handed set. In the S/C frame, +Z is along the spin axis or S/C-Sun line, +Y is orthogonal to +Z and parallel to the deployed MAG boom, and +X completes the right-handed set. Note that both +z and +Z point along the spin axis. The instrument frame angles elevation (θ), and azimuth (φ), and the S/C frame angles spin (β), and polar (α) are defined in Table 3 and their relationships are illustrated in Fig. 3a. Figure 3 b,c show the CoDICE sky coverage in one S/C spin. CoDICE-Lo ESA has an instantaneous FOV of 6° in elevation × 360° in azimuth and covers ∼1.8 π sr in a single S/C spin, while the 12 10° in elevation × 16° in azimuth collimators of CoDICE-Hi cover 2.1 π sr in each S/C spin.

Table 3 Definition of CoDICE frame and S/C frame angles and their relationships

Angle	Definition	Coordinate System
Azimuth (**φ**)	Clockwise angle from the +z axis when viewing the y-z plane from the +x direction (i.e., when looking towards the instrument from the spacecraft)	Instrument
Elevation (**θ**)	Angle out of the CoDICE-Lo FOV plane, with +θ in the +x (towards the S/C)	Instrument
Polar (**α**)	Angle from +Z (S/C spin axis) towards the center look direction of detector (APD/SSD)	Spacecraft
Spin (**β**)	Angle from S/C spin phase 0° to the center look direction of detector (APD/SSD)	Spacecraft

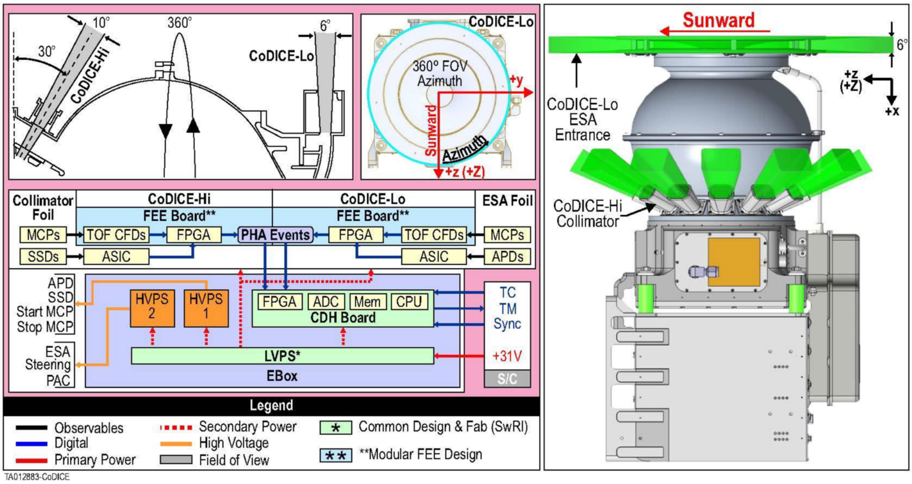

Fig. 2 CoDICE Block diagram along with FOVs in the instrument frame relative to the S/C spin axis

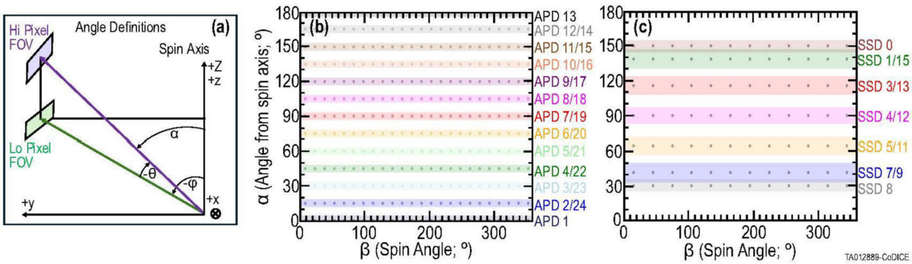

Fig. 3 a) Instrument frame angles and their relationship to spacecraft frame angles. b, c) CoDICE-Lo and -Hi sky coverage in one S/C spin

3.2 CoDICE Sensor & Electronics

Figures 2 and 4 show that CoDICE comprises four major subsystems, namely, 1) the ESA; 2) the TOF/E; 3) the Front-End-Electronics or FEE; and 4) the Electronics Box (Ebox).

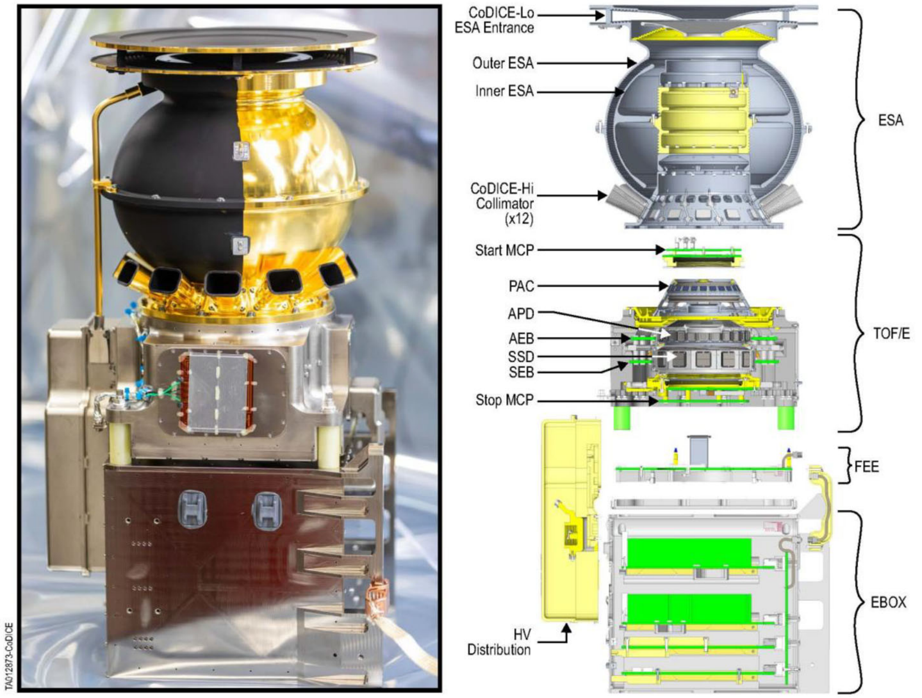

Fig. 4 CoDICE photograph and cross-section cut showing the four major subsystems in an expanded view

3.2.1 ESA Subsystem

The ESA subassembly comprises the CoDICE-Lo ESA and the 12 CoDICE-Hi collimators and apertures. The ESA has an outer electrode with an entrance electrode (Outer ESA) and an inner electrode (Inner ESA) that are both designed and tested to operate independently up to -14.1 kV and enable CoDICE to reduce its geometric factor during high count rate periods (Sect. 5.2 mentions "geometric factor"). The Inner ESA is a single machined part, while the Outer ESA comprises upper and lower sections bolted together to form the entrance electrode and the outer electrode. Both the Inner and Outer ESAs are concentric toroids with active surfaces scalloped to attenuate UV and minimize scattering. Ebanol-C coating was applied to internal parts of the ESA to reject UV. Prior to the Ebanol-C conversion, the parts were electroless nickel plated, copper plated, and then gold plated in all areas that Ebanol-C was not required. The upper portions of the ESA and the anti-sunward facing side of the outer ESA are blackened to maintain the sensor temperature within nominal operating range of the APDs (see Sect. 3.2.5).

Each of the 12 CoDICE-Hi collimator assemblies has an acceptance angle of 10° elevation $\times$ 16° azimuth. The interior surfaces are scalloped and Ebanol-C coated. UV rejection is accomplished using 2 foils attached to 70 lines-per-inch (LPI) grids. The external foil is 100 nm aluminum and the internal foil is 50 nm aluminum with 50 nm polyimide.

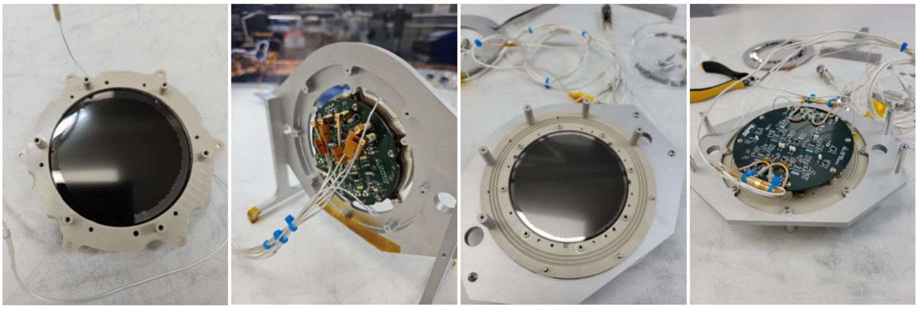

Fig. 5 Flight units of the front and back of the CoDICE START (left) and STOP (right) MCP sub-assemblies

3.2.2 TOF/E Subsystem

The TOF/E subsystem includes a Post Acceleration Region (PAC) assembly, the START and STOP detector assemblies, 24 APDs and the APD Energy Board (AEB) for CoDICE-Lo, and 12 SSDs and the SSD Energy Board (SEB) for CoDICE-Hi.

1. The PAC Assembly The PAC assembly comprises a foil mount, with 24 thin START carbon foils each with area ~42.4 mm^2 for CoDICE-Lo, 12 thin START carbon foils each with area 95.5 mm^2 for CoDICE-Hi, two electron steering electrodes, and an insulator. The foil mount and START C foils are at −15 kV potential and the steering electrodes operate at −13.7 kV. The carbon foils are floated on 333 LPI grids that are spot welded to stainless steel frames.

2. START and STOP MCP Assemblies: Mechanical, Electro-Optics, Biasing, and Readout CoDICE employs two MCP Z-stack subassemblies—START and STOP—each mounted in an alumina carrier on PEEK stand-offs within seam-welded shield cans (see Fig. 5). A single star-point chassis bond serves both cans and all high-voltage (HV) returns. SHV feedthroughs deliver graded biases; anode signals are conveyed over short RG-178 micro-coax with the outer braid tied to chassis. Constant-fraction discriminators (CFDs) in the FEE-START and FEE-STOP modules generate timing outputs for the Lo-FEE and Hi-FEE FPGAs (see Sect. 3.2.3.1). A controlled radio frequency (RF) return between chassis and analog ground (AGND) is provided by a 0.027 μF bond.

START Optics and Stack Downstream of the entrance foils, a field-defining optics grid is held at −3.5 kV. Two upstream steering electrodes at −15 kV and −13.5 kV guide the electron trajectories into the START MCP while minimizing backscatter. Figure 5 (left) shows that the START Z-stack uses three plates graded at $\Delta V = 0.7$–1.0 kV per plate (total ≈2.1–3.0 kV); the front face is −2.8 to −3.4 kV and the back/anode plane is set to ~0 V. The anode comprises a one-dimensional 24-element position-sensitive delay line flanking a central collection strip. Both delay-line ends and the central strip are near 0 V DC and are AC-coupled through 27 nF/200 V capacitors into the first preamplifier stage; 10 MΩ bleeders from each node to AGND set the DC reference without shunting fast charge. The first preamplifier stage is chassis-referenced; a second stage is AGND-referenced. CFDs receive Lo START A/B (Fig. 6, delay-line ends), and Hi START (central strip).

Position Sensing Delay-Line The START delay line required five PCB iterations (Fig. 7, top) to meet the spatial and timing specifications. Early efforts showed (1) inter-turn crosstalk from inadequate spacing and weak ground fencing, (2) ringing caused by impedance steps, stubs, and via transitions, and (3.) broken return paths across split planes.

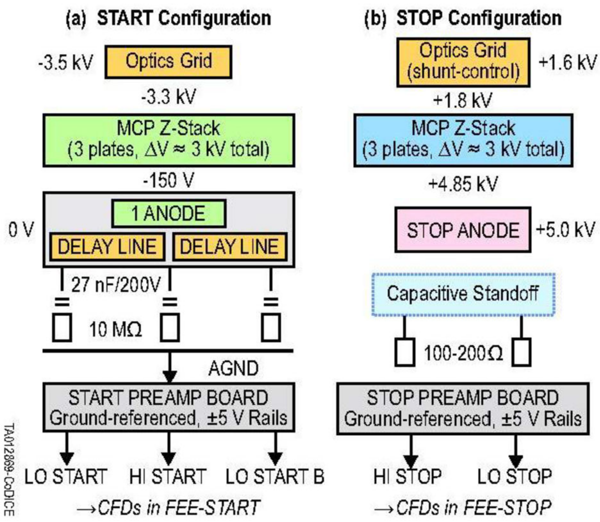

Fig. 6 Anode readout and HV bias configuration for a) START and b) STOP MCP detectors. The START configuration uses a ground-referenced delay-line anode (0 V) with AC-coupling through 27 nF/200 V capacitors and 10 MΩ bleed resistors. The optics grid operates at −3.5 kV with the MCP stack providing ∼3 kV gain. STOP employs a high-voltage anode at +5.0 kV requiring capacitive standoff and series damping (100–200 Ω) for ground-referenced readout. The optics grid operates at +1.5–1.6 kV with shunt control. Both systems share a common chassis star-point ground with 0.027 μF chassis-to-AGND coupling for RF return

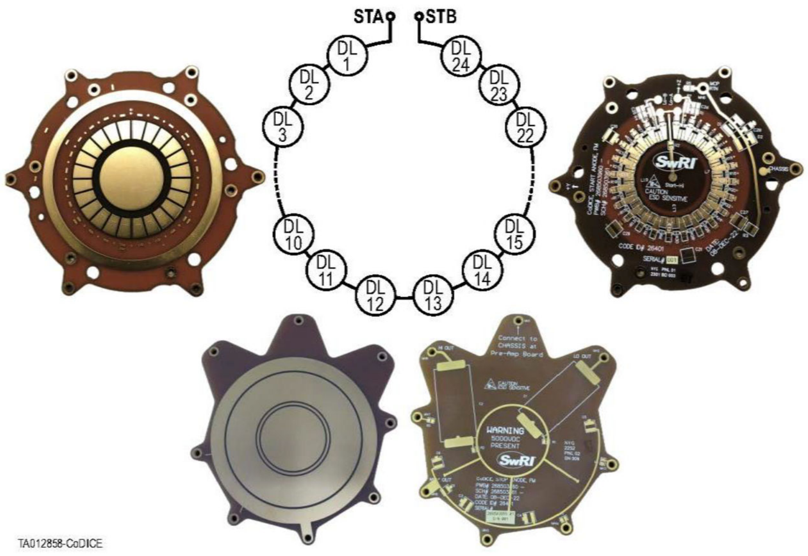

Fig. 7 Top: Rear, pad layout, and front of the START anode, depicting the position sensing delay-line. Bottom: Rear and front of the STOP anode

The final layout employs controlled-impedance microstrip (∼50 Ω), continuous ground under the serpentine, dense via-fencing (≈2–3 mm pitch), symmetric stub-free fan-out to matched 50 Ω terminations, and strict length matching. The realized propagation constant is ∼5–8 ns cm^{-1}; differential timing walk is <200 ps across the operating rate, and flat-field calibration yields ∼0.5–1.0 mm FWHM spatial resolution.

STOP Optics and Stack A downstream accelerator grid is biased to +1.5 to +1.6 kV (trimmed through a shunt-control divider) to inject electrons into the STOP Z-stack (Fig. 6, right, Fig. 7 bottom). Plates are graded at ΔV = 0.7–1.0 kV per plate, placing the front face

Fig. 8 An APD (top left) and an SSD (bottom left), and flight units of the CoDICE AEB (middle), and SEB (right)

at approximately +4.3 to +4.9 kV and the STOP anode at +5.0 kV. Because the anode rides at HV, signals are AC-coupled across a capacitive standoff to ground-referenced preamplifiers; series damping (≈100–200 Ω) and bias-tee partitioning suppress dV/dt-induced ringing. CFDs provide Hi STOP and Lo STOP logic timing.

Grounding, Cross-Talk, and Noise Control Both START and STOP shield cans bond to a single chassis star point, and all HV returns land at this node. AGND is not hard-tied to chassis; a 0.027 μF capacitor near the preamp/FEE interface defines the high-frequency return while avoiding DC ground loops. HV lines are RC-filtered at/inside each feedthrough to confine displacement current and prevent the HV wiring from coupling pulses between bays. Copper partitions and anode-board guard rings, tied to the can, reduce inter-assembly capacitance. Harnesses are segregated and cross at 90° only where unavoidable; all anode paths use 50 Ω RG-178 with braid grounded at entry and true 50 Ω terminations to eliminate reflections. Three START and two STOP test-pulse injection lines exercise the full signal path and provide a reproducible reference for the instrument's coupling floor, assisting data users in distinguishing physical coincidences from artifacts.

3. APD and SSD Energy Boards (AEB & SEB) APDs in the AEB (Fig. 8) provide energy measurements from 1 keV to ∼250 keV for CoDICE-Lo and SSDs in the SEB (Fig. 8) measure ions from ∼100 keV to 160 MeV in CoDICE-Hi.

Both the AEB and SEB use two 32-channel ASICs, each is a front-end integrated circuit designed for low-noise charge signal acquisition and processing. Each channel integrates a charge preamplifier with selectable polarity and a 200 fF test capacitor, followed by a fifth-order shaping amplifier with selectable peaking times of 500 ns, 1 μs, 2 μs, or 4 μs. The channels also feature a bandgap referenced baseline stabilizer (≈250 mV), selectable gain settings (14.25, 28.5, and 57 mV/fC), a peak amplitude detector with analog memory, and a single-threshold discriminator. Signal readout is managed through shared 32:1 multiplexers for the peak detector and analog monitor, supported by analog output buffers, two 10-bit DACs (for threshold and test pulse amplitude control), internal bias generators, and read/write logic. The ASIC operates at approximately 166 mW (4 mW per channel plus 38 mW shared circuitry) and is fabricated using a 0.25 μm complementary metal-oxide semiconductor (CMOS) process with 2.5 V operation, 1-poly, 5-metal layers, MiM capacitors, and silicide-blocked resistors. The physical layout measures 4922×4922 μm^2, with the final die cut size to be determined by Metal Oxide Semiconductor Implementation Service (MOSIS). The device includes 80 pads, each 68 × 68 μm^2 with a 220 μm pitch. The design

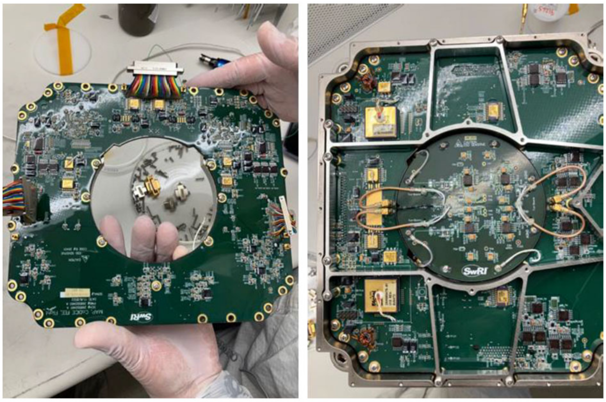

Fig. 9 The FEE board

emphasizes compactness, configurability, and low-power operation, making it well-suited for high-density sensor readout applications.

The AEB uses 24 silicon APDs from Hamamatsu each with a 3×5 mm^2 active area and $\sim$300 μm thickness. Each detector is reverse-biased at approximately 500 V, with closed-loop adjustment from four on-board thermistors to keep gain stable over temperature. A dedicated low-pass filter cleans the high-voltage bias to preserve energy resolution. Each APD signal is split by a dual-range charge-division network, high and low, to extend the dynamic range and prevent ASIC saturation. The split yields 48 analog inputs routed to two ASICs, 24 lines per device. The SEB uses 12 single-pixel silicon detectors from Mirion Technologies with a 15×15 mm^2 active area, $\sim$700 μm thickness, and an entrance window <50 nm. Each detector is reverse-biased at 190 V, with a low-pass filter on the high-voltage supply to reduce noise. To expand the measurable energy range without saturating the front end, each SSD employs a three-range charge-division network—low, mid, and high—mapping six detectors per ASIC into 18 analog inputs. The SSDs are mounted on a customer-supplied carrier and wire-bonded by Mirion.

3.2.3 FEE Board

Figure 4 shows that the Front-End-Electronics (FEE) board resides under the sensor. The FEE (Fig. 9) receives the Lo-STARTA, Lo-STARTB, Lo-STOP, and APD energy signals from CoDICE-Lo and Hi-START, Hi-STOP and SSD energy signals from CoDICE-Hi and then transmits the processed event data listed in Table 4 to the CDH FPGA (see Sect. 6.3) for further processing.

1. TOF CFDs The constant fraction discriminator (CFD) circuit interfaces with the TOF signals from the START and STOP MCPs and is designed to reduce the TOF "walk" that arises from different signal amplitudes on the inputs. The circuit includes a preamplifier stage that buffers and amplifies the MCP pulses, making it suitable for input pulse amplitudes ranging from 10 mV to 500 mV. In the CFD stage, the signal is split into two paths: one path is delayed and inverted, while the other is amplified by a factor of two. These two signals are then compared to generate a timing output that is largely independent of the input pulse amplitude, significantly improving timing resolution. The CFD achieves a timing accuracy of 250 ps standard deviation across varying temperatures and pulse heights. To reduce sensitivity to noise, the CFD includes a programmable threshold level, controlled by a DAC

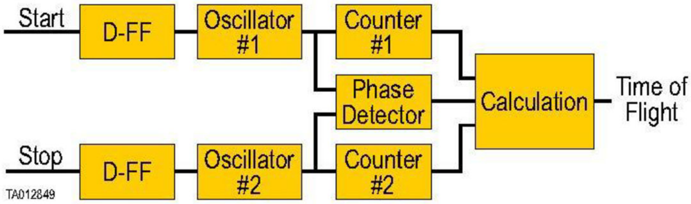

Fig. 10 Vernier TDC Method

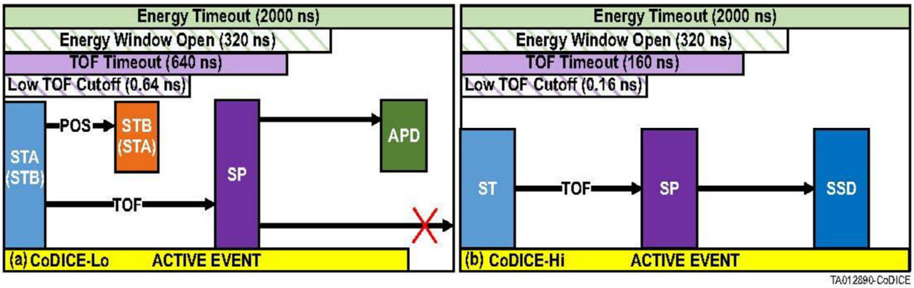

Fig. 11 PHA event timing for a) CoDICE-Lo and b) CoDICE-Hi

managed by the FPGA. The circuit also includes a stim input, allowing the FPGA to inject test pulses for end-to-end functionality checks. Ultimately, the CFD converts analog MCP pulses into clean digital timing signals that are sent to the FPGA for precise time-to-digital (TDC) conversion.

2. FPGA The FEE CoDICE-Lo and CoDICE-Hi FPGAs are nearly identical except for slightly different event processing as described below. One common function performed by both FPGAs is the ability to measure the delay between two pulses, e.g., from the delay line anode for CoDICE-Lo and between the START and STOP signals for both CoDICE-Lo and CoDICE-Hi. The FPGA digitizes the time between each pulse using a TDC based on the Vernier TDC method (Fig. 10, Hua and Chitnis 2022). It uses two oscillators of slightly different frequencies to measure the time difference between the pulses. The timing pulses use an edge-triggered latch – data flip-flop (D-FF) – to start the oscillators. The TDC is able to achieve a resolution of 10 ps, but the lower bits of the resulting measurement are dropped to retain 0.64 ns for TOF measurements and 0.32 ns for Position in the CoDICE-Lo FPGA, and 0.16 ns for TOF measurements in the CoDICE-Hi FPGA.

The FPGA provides various timers (see Fig. 11) for receiving valid TOF and Energy events for CoDICE-Lo and CoDICE-Hi. The timers begin at the receipt of a START pulse, which marks the beginning of an active PHA event. The PHA event ends with a measured TOF being less that the Low TOF Cutoff threshold, receipt of an APD/SSD energy occurrence, or expiration of the Energy Timeout period set at 2000 ns. The Energy Timeout serves as the overall PHA Event timeout since it terminates the event. Therefore, a valid TOF is defined as a START-to-STOP delay between the Low TOF Cutoff and TOF Timeout expiration. PHA events with TOF values below the Low TOF Cutoff threshold are deemed invalid and discarded.

Table 4 PHA events processed by the FEE FPGA and transmitted to the CDH FPGA; '+' = AND; '( )'= OR

Event Type	CoDICE-Lo		CoDICE-Hi	
Valid TCR	STA+STB+SP+APD	Position, Corrected TOF, Energy	ST+SP+SSD	TOF, Energy
DCR (TOF only)	STA+STB+SP	Position, Corrected TOF	ST+SP	TOF Only
Energy events	STA(B)+SP+APD	Raw TOF, Energy		
	STA+STB+APD	Position, Energy	SP+ SSD	STOP, Energy
	STA(B)+APD	Energy	SSD	Energy

3. CoDICE-Lo FPGA Processing The CoDICE-Lo FPGA receives two signals from the START Pre-Amplifier Board (PAB): Lo-START – A (STA) and Lo-START – B (STB); one signal from the STOP PAB: Lo-STOP (SP); and APD energy event notifications from the two ASICs on the AEB.

The FPGA uses the TDC time value to measure the delay between STA and STB pulses (Fig. 7) and determine which of the 24 anodes in the delay line was triggered. Each anode adds ∼1.1 ns of delay as the signal traverses through the delay line. Thus, the delay between the STA and STB pulses determines the anode position, defined as the delay-line position index (DL). Furthermore, a positive delay indicates anode positions DL1-DL12 were triggered while a negative delay indicates anode positions DL13-DL24. Each APD has a corresponding low and high gain channel into the ASIC (see Sect. 3.2.2; AEB). A high energy ion could trigger both ASIC channels, in which case the FPGA determines the channel to report the energy by comparing the high gain channel energy to the high gain threshold provided by FSW for the associated APD. An energy value greater than or equal to this threshold deems the channel as saturated, in which case the energy of the low gain channel is reported with no comparison to a saturation threshold. A high gain energy below the threshold is reported and the associated low gain channel is ignored. If the low gain channel isn't triggered, then the high gain energy is reported even if it exceeds the saturation threshold. In cases where more than one detector triggers the ASIC, the FPGA reports the energy of the first detector reported and sets the 'multiple' bit in the science event packet to indicate that multiple detectors coincidentally triggered the ASIC.

Calibration was used to determine the actual delay time boundaries for each anode position which are stored in a Look-Up Table (LUT) within the FPGA and used for converting the measured TDC time to the corresponding anode position. The LUT also provides a TOF correction as follows. The TOF TDC time measurement begins with whichever occurs first of the STA or STB pulses. The Position LUT mentioned previously accomplishes this by providing a TOF correction that corresponds to the delay of the commencing START pulse through the delay line. This TOF correction is added to the raw TOF measurement to provide a corrected TOF measurement. Note this correction is only available when a valid Position is measured. Otherwise, no correction is applied and the raw TOF measurement is provided to the event processor.

Table 4 shows the CoDICE-Lo PHA events identified as triple coincidence (TCR: STA+STB+SP+APD), double coincidence (DCR: STA+STB+SP), and energy events (APD, only one or two of STA, STB, SP) that are transmitted to the CDH. All instrument rate counters are also incremented with each event type.

4. CoDICE-Hi FPGA Processing The CoDICE-Hi FPGA receives one START (ST) signal from the START PAB, one STOP (SP) signal from the STOP PAB, and SSD energy event notifications from the SEB. To cover the required energy range, each SSD has a low, medium,

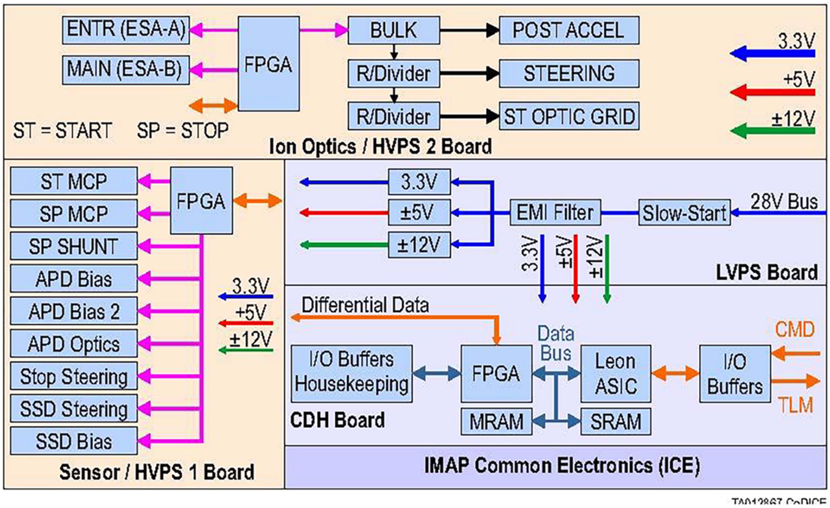

Fig. 12 CoDICE Ebox

Fig. 13 From left, CoDICE HVPS 1, HVPS 2, LVPS, CDH, and the Ebox

and high gain channel into the ASIC (see Sect. 3.2.2; SEB), which are processed in identical fashion as the APD low and high signals described above. Table 4 also shows the CoDICE-Hi PHA events identified as triple coincidence rates (TCR; ST+SP+APD), double coincidence (DCR: ST+SP), and energy events (SSD only or ST + SSD only) that are transmitted to the CDH. All instrument rate counters are also incremented with each event type.

3.2.4 Electronics Box (Ebox)

The CoDICE electronics box (Ebox, Fig. 12) comprises the following subassemblies (Fig. 13) 1) Low Voltage Power Supply (LVPS); 2) Command and Data Handling (CDH) or Processor Board; 3) Sensor HVPS or the High Voltage Power Supply 1 (HVPS); 4) Ion Optics or HVPS 2; 5) Backplane; and 6) Low voltage terminal block assembly. CoDICE uses the Backplane, CDH, and LVPS from the IMAP Common Electronics (ICE) developed at SwRI for several IMAP instruments, namely, IMAP-Lo (Schwadron et al. 2025), IMAP-Hi (Funsten et al. 2026), SWE (Skoug et al. 2026), and GLOWS (Bzowski et al. 2025).

The LVPS interfaces with the spacecraft via a nine-pin D type connector to accept +31 V nominal spacecraft primary power to create secondary voltages (+3.3 V, ±5 V, ±12 V) for all CoDICE subassemblies. The CDH board interfaces to the spacecraft RS-422 data bus via a 9-socket MDM type connector for all S/C commands and instrument telemetry. The

CDH 1) provides a centralized system for command, monitoring, and control; 2) acquires, processes, and packetizes all detector data; 3) provides temperature, current, and voltage monitoring of the HVPSs, LVPS, and the sensor; and 4) distributes HVPS Safing.

HVPS 1 or Sensor HVPS has four HV converters, namely, 1) Sensor bulk; 2) START MCP; 3) STOP MCP; and 4) APD Bias. The HVPS 1 Bulk supply produces a steady output voltage of +6000 V. The bulk output feeds directly into the STOP Steering regulator (+3200 V nominal, HV optocoupler based) which is resistor divided to produce the SSD Steering voltage (+1600 V nominal). The sensor bulk provides +670 V from a tap on the multiplier/filter to three additional outputs. One of these – SSD Bias – also has an HV optocoupler based regulator. The remaining two – APD Optics and SSD Lens – are derived from resistive dividers. The START MCP supply produces an output voltage programmable from zero to -3400 V, with current capability is upto 120 μA. The STOP MCP supply produces an output voltage programmable from zero to +5000 V, with the current capability up to 120 μA. The MCP Back voltage is set to a fixed voltage from +1600 V by using a shunt HV optocoupler. This voltage increases as the STOP MCP voltage increases until it reaches +1600 V, then it is regulated to a fixed +1600 V as the STOP MCP voltage continues to increase. The APD Bias supply produces a programmable output voltage of zero to +650 V. There is a slave APD Bias 2 supply producing zero to $\sim$ +600 V to bias three APDs that measure the solar wind. Since APD Bias 2 is a regulated voltage from APD Bias 1, it cannot generate a voltage greater than the programmed APD Bias 1 voltage.

HVPS 2 Bulk supply or Ion-optics HVPS produces a programmable output voltage (0 to $-15{,}500$kV) with a nominal voltage of -15 kV and current capability up to 200 μA. The output of this Bulk supply feeds directly into the entrance ESA and the main ESA HV optocoupler based negative polarity stepping power supplies. This Bulk supply also feeds a resistive divider which provides the PAC output (nominal -15kV), the Steering output (nominal -13,240 V) and the START Optics Grid (nominal -2647 V).

The backplane routes 1) secondary power from the LVPS to all other subassemblies, and 2) command and telemetry from and to the CDH. All electrical interfaces within the Ebox are via cPCI connectors. The low-voltage electrical interface to the sensor section is via a pigtail two-row 51-pin MDM type connector between the Ebox and the FEE housed in the Sensor.

The low-voltage terminal block assembly provides lower-level high voltage termination via high-voltage pigtails exiting directly from HVPS 1 and 2 at the Ebox exterior prior to being integrated with the sensor assembly. The higher voltages were terminated after the sensor section was integrated with the Ebox. The lower-level high voltages include Ion-Optics HVPS voltages, START Optics Grid, and Sensor HVPS voltages: START MCP, STOP Steering, STOP Anode, START Anode, APD Optics, SSD Lens, SSD Steering, STOP Grid, and STOP MCP Back.

3.2.5 Thermal Design

The multiplication factor or gain and the energy resolution of a given APD varies with bias voltage and temperature (Ogasawara et al. 2012). This inherent APD feature necessitates that the APDs' operating temperature remains within -20 °C to +40 °C. Maintaining the APDs within this range also increases their overall lifetime. To achieve this and enable nominal performance over the two-year duration of the prime mission, CoDICE thermal design comprises a two-zone system separated into 1) the electronics housing, and 2) the sensor or instrument portion.

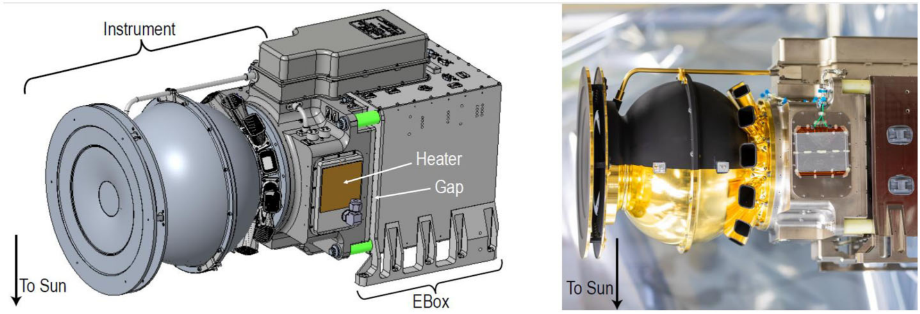

Fig. 14 (Left) Two thermal zones for CoDICE. (Right) Photograph of CoDICE

1. Electronics Housing The electronics housing or Ebox (Fig. 14) is thermally coupled to the spacecraft deck which serves as a heat sink. The deck temperature ranges were evaluated from 55 °C to −20 °C and all components meet the EEE-INST-002 temperature derating standard. The CoDICE electronics boards were designed and their layout was determined after taking account of the following thermal properties and constraints, namely, 1) the amount of significant copper layers, 2) component placement (closer to the chassis interface is colder), and 3) electrically insulative materials. When considering high voltage standoffs for a robust optocoupler system, the HVPS 2 thermal design enhancement consisted of employing thermal conductive Shapal instead of thermally insulative PEEK.

2. Instrument The second thermal zone houses the instrument, which is separated physically from the Ebox by a gap and mounted to it with bolts and four thermally insulative G10 spacers, shown in green in Fig. 14. Additionally, to reduce heat transfer across this boundary, low conductive materials like PEEK were used for the covers that bridge the zones at the top of the Ebox. Surface treatments were also considered to minimize radiative coupling between the two zones. Electroless nickel plating was used on the opposing faces at the boundary. One side of the ESA faces the Sun and is largely covered with multi-layer insulation (MLI) to reduce the solar influx. The opposite face is painted black and serves as a radiator for passive heat rejection to maintain the overall sensor within the operating temperature range of the APDs, especially in the hot thermal case. The large size of this radiator necessitated the use of dual-element patch system heaters (brown in Fig. 14) on either side of the instrument in the cold and survival operation modes. The operational heaters are software controlled, while the survival heaters are thermostatically controlled. The cold setpoints for the operational heaters were artificially decreased to ensure the operation and survival control schemes are well separated given the overlap between the APD operational and survival limits.

4 Sensor Model

Figure 1 illustrates trajectories of primary ions (depicted in brown) and secondary electrons (shown in blue) calculated using SIMION numerical simulations. We implemented complete 3D designs of CoDICE, including asymmetric parts and serrating structures, to model the charged particle trajectories accurately. Sample electric equipotential lines within the TOF/E and ESA subsystems, represented by thin red lines with 600 V increments, are also shown in Fig. 1. The PAC is set at −15 kV to reduce the velocity straggling of the primary ions passing through the thin carbon foils. CoDICE primarily uses neutral particles (n_0) to trigger the energy signals so that the read-out electronics are kept at the ground potential. Although this technique does not affect energy signals from the lower energy ions (<10 keV/nuc), the higher-energy ions can produce secondary peaks separated by ∼15 keV, which is greater than the APD energy resolution (Fig. 20d, Ogasawara et al. 2012). We characterized this effect during the TOF/E calibration (Table 5) and will use the results to validate the flight data.

Since CoDICE-Lo and CoDICE-Hi share the START and STOP MCPs for the TOF measurements, ions entering the instrument in either aperture can generate secondary electrons that deviate from ideal paths and land in non-designated locations on the START and STOP MCPs, thus cross-contaminating the TOF signals within the event timeout window. The overall electrode layout and voltages were modeled and selected to minimize dispersions in both, the electron landing positions and travel-time. In the model, secondary electrons are produced from four separate locations in cosine distributions in angle with 1–5 eV core energy and a long tail beyond 30 eV (Allegrini et al. 2016). The integrated probability of landing locations for START/STOP electrons, shown in Fig. 15 a,b, are used to estimate the physical cross talk probabilities for both CoDICE-Hi and -Lo as shown in Figs. 15 c,d. The integrated rate (R) is given by:

$$R(r) = \frac{1}{C_d} \int_{r_0}^{r} C_i \Delta r \tag{1}$$

where $r_0 = 0$ is the center of the anode and r is the radial distance from $r_0 = 0$. C_d denotes the total detected counts and C_i the counts in the radius bin. Based on this result, the gray areas in Figs. 15a and 15b were set to separate the inner and outer annulus of the MCP anodes. Figure 15 c,d show key secondary electron properties. The angular dispersion of the Lo-START signals is calculated to estimate the position resolution of the delay line anode location. The delay-line anode has 24 discrete conductive pads connected through LC chains to create ∼2 ns delay per each 15° azimuthal location. The expected 1σ angular dispersion of the secondary electrons was 4.6°. The electron TOF distributions for all four locations are also shown in Fig. 15. The Lo-STOP signal has the largest timing dispersion of 0.7 ns, while the 1σ dispersions for other locations were ∼0.3 ns. The secondary electrons in these calculations are uniformly created throughout the active surface (i.e., carbon foils and silicon detector surfaces) using the energy/angular distributions discussed above.

5 Calibration and Cross-Calibration

5.1 Calibration Procedures

CoDICE calibration was carried out separately for the ESA and TOF/E subsystems and then for the full sensor assembly to ensure functionality and performance characterization. The energy calibration used radioactive sources to evaluate the AEB and SEB performance and is critical for obtaining the absolute energy response. The TOF/E subsystem was also calibrated using higher energy singly charged ions without the ESA since the upper energy limit of the ESA is 80 keV/q. Finally, the full flight sensor was calibrated to evaluate end-to-end performance and functionality. Table 5 summarizes the calibrated parameters (species, energies, locations, and angles). Table 6 provides the definitions of detector IDs in terms of instrument azimuth angles and instrument-reported rate index. Azimuth 0 is in the solar wind (SW) or sunward direction and Azimuth 180 is in the anti-sunward (NSW) direction.

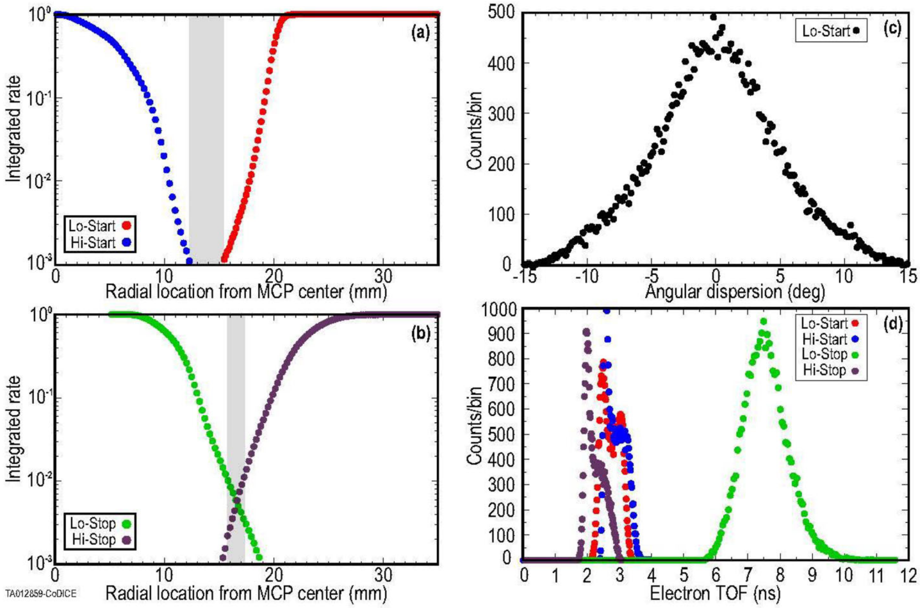

Fig. 15 Probability of secondary electron landing locations for a) START MCP and b) STOP MCP for the flight configuration. The gray area separates the inner and outer anodes of MCP read out system. c) Angular distributions of the START signals. d) TOF distributions of secondary electrons for all four locations

We used two key San Antonio SwRI laboratories for these calibration activities: the plasma ion calibration chamber (H30; McComas et al. 2009) and the high-energy particle accelerator (H19). H30 is equipped with a 4-axis positioning system, capable of mounting an 8-cubic-feet instrument with high precision. The plasma source provides an ion beam with energies from 1 to ∼30 keV/q and species from H to Ar. The H19 source provides singly charged H to Kr ions up to 350 keV/q. The H19 vacuum chamber is maintained under mid 10^{-8} Torr, and together these two facilities provided extensive capabilities for calibrating and validating the instrument performance.

5.2 Electrostatic Analyzer Performance

The CoDICE-Lo ESA performance was investigated using H30. The positioning system controlled the sensor attitude with 5 μm and 0.01° accuracy. An axisymetric performance was assumed about the instrument rotation axis (-x in Fig. 1). Therefore, the horizontal angle of the sensor aperture was ignored, and only the elevation angle was evaluated for multiple azimuth locations, which also corresponds to location of each APD in the TOF/E subsystem (Table 6). For CoDICE-Lo, the azimuth angles are not fully covered due to limitations in the size of the APDs and internal structures that block secondary electrons. Figure 16 shows the double (DCR, orange) and triple coincidence rates (TCR, blue) for 1° azimuth angle scans from −180° to 180° using proton beams at two energies, namely, 43.5 keV (top) and 16.5 keV (bottom). The periodic patterns in the DCRs and TCRs highlight the sensor's angular response reflecting internal carbon foil structures.

Table 5 Summary of CoDICE calibration efforts

	Cal. Type		Species	Energy	Az locations*	El angle
CoDICE-Lo	Energy	AEB only	Fe-55, Am-241	5.9 keV (γ), 14–60 keV (γ)	1–24, 15° steps	0°
	TOF-E	No ESA	H, He, N, Ne, Ar, Kr	5, 15, 40, 100, 200, 300 keV	1–24, 15° steps	0°
		With ESA	H, H2, He, N, Ne, Ar	5–80 keV (25 selected over 1–80 keV/nuc)	1–24, 15° steps	0°
	Full	Energy-Angle scan	H	4, 16 keV	1,3,9,11,13, 21,23	−3° to 3°, 0.5° steps
		Energy-Angle scan	H, He	1, 2, 4, 6, 10, 16, 24, 43.5, 71.5 keV	1, 15	−3° to 3°, 0.5° steps
		Energy-Angle scan (Low-GF)	H	4, 16 keV	1, 15	−3° to 3°, 0.25° steps
		Fine angle scan	H, He, Ne	5, 16.5, 43.5 keV	1–24, 2° steps	0°
CoDICE-Hi	Energy	SEB only	Am-241, Th-228, Cf-252	59.5 keV (γ), 5–9 MeV (α), 90–130 MeV (fission)	0–15, 30° steps	0°
	TOF-E	No UV foil	H, He, N, Ne, Ar, Kr	50, 100, 150, 200, 225, 250, 275, 300 keV	0–15, 30° steps	0°
		With UV foil	H, He, Th-228	100, 150, 200, 250, 300 keV (beam), 5–9 MeV (α)	0–15, 30° steps	0°
	Full	Fine angle scan	He, Th-228	300 keV (beam), 5–9 MeV (α)	0, 15	−10° to 10°, 1° steps
					0, 1, 7, 8, 15, 1° steps	0°

*Az location is indicated by the rate index in Table 6.

The energy geometric factor (G_E) of an ESA, in units of cm^2 sr eV/eV, is given by:

$$G_E = \frac{\Delta\varphi}{E_0} \sum_m \sum_n \frac{C_{mn}}{\Phi} E_m \cos\theta_n \Delta E \Delta\theta \tag{2}$$

$\Delta\varphi$ – is the azimuthal angle range of interest, E_0 – the reference energy, E_m – the mth energy step, θ_n- the nth elevation angle, ΔE – the energy step, $\Delta\theta$ – the elevation angle step, Φ – the incident beam flux, and C_{mn} – the sensor count rate at the given step. G_E is estimated by summing over the relevant increments, weighted by their respective counts for a given incident particle flux. When evaluating the beam flux, an Absolute Beam Monitor (ABM, Funsten et al. 2005) was used to measure efficiency independent values by using following:

$$C = \frac{C_A C_B}{C_{AB}} \tag{3}$$

Table 6 CoDICE APD and SSD detector ID's, azimuths, and rate index in the instrument coordinate system. For CoDICE-Lo the APDs are also mapped to the delay-line position index (DL)

CoDICE-Lo				CoDICE-Hi		
Channel	Azimuth	Position (DL)	Rate Index	Channel	Azimuth	Rate Index
RH3	0	1	1	LH1	0	8
RH4	15	2	2	LH2	30	9
RH5	30	3	3	LH3	60	11
RH6	45	4	4	LH4	90	12
RH7	60	5	5	LH5	120	13
RH8	75	6	6	LH6	150	15
RH9	90	7	7	RH1	180	0
RH10	105	8	8	RH2	210	1
RH11	120	9	9	RH3	240	3
RH12	135	10	10	RH4	270	4
LH1	150	11	11	RH5	300	5
LH2	165	12	12	RH6	330	7
LH3	180	13	13			
LH4	195	14	14			
LH5	210	15	15			
LH6	225	16	16			
LH7	240	17	17			
LH8	255	18	18			
LH9	270	19	19			
LH10	285	20	20			
LH11	300	21	21			
LH12	315	22	22			
RH1	330	23	23			
RH2	345	24	24			

$$\Phi = \frac{C}{A} \tag{4}$$

where C is the incident rate, A – the ABM acceptance area ($\sim$1 cm^2), $C_A = \varepsilon_A C$ – the count rate on detector A with efficiency ε_A, $C_{B\,=}\ \varepsilon_B C$ – the count rate on detector B with efficiency ε_B, and $C_{AB} = \varepsilon_A \varepsilon_B C$ – the A and B coincidence rate. During CoDICE calibration, we fixed the beam energy of the ions and simultaneously scanned the ESA voltages (both entrance and main electrodes) around the passbands. The elevation angles were physically altered using the chamber's motion stage. Negative elevation angles correspond to particles arriving from above the ESA dome and positive elevation angles to those from below. The beam flux was recorded before and after each angular step with a complete energy scan.

Count rates at the low-energy portion of the ESA sweep are expected to be higher, and since excessive count rates can affect the lifetime of the MCP and APD detectors, the instrument uses a Reduced Geometric Factor Operation (RGFO, Sect. 6.4.3) mode once a configurable count rate threshold is reached. In this mode, the Outer ESA voltage is set according to the 128-step sweep, but the Inner ESA voltage is set to a fraction of the Outer ESA voltage. This reduces the number of ions that can pass through the ESA and reduces the count rate. In the RGFO mode, the entrance electrode voltage was reduced by the factor

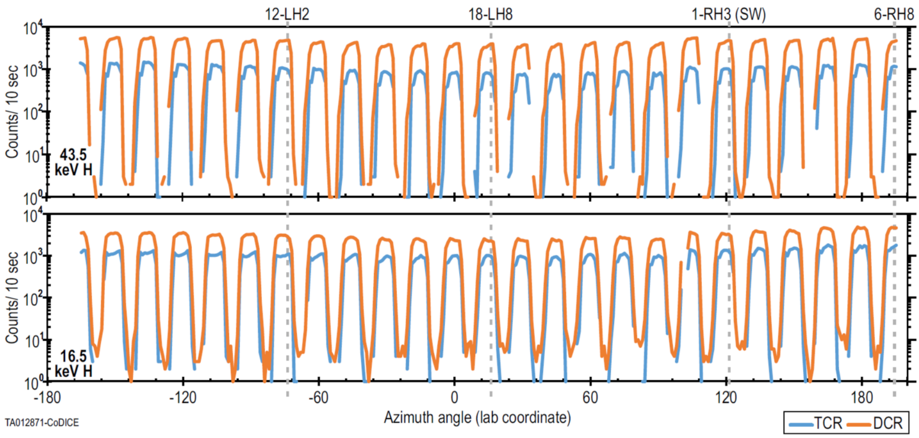

Fig. 16 The sensor double coincidence rate (DCR) and the triple coincidence rate (TCR) responses with fine (1°) azimuthal angle scan for the 43.5 keV and 16.5 keV proton beam. The solar wind sector is at +120° in this laboratory coordinate. The vertical axis shows the accumulated counts within 10 seconds for all channels

Table 7 Summary of reduced geometric factor mode (RGFO) performance for CoDICE-Lo evaluated using 16 keV protons. G_E units are cm^2 str eV/eV. RGFO mode is achieved by using factor 0.7 ratio between the entrance or ESA-A and main or ESA-B voltages

Sector		Type	K-factor (RGFO)	K-factor (Normal)	G_E (RGFO, R= 0.7)	G_E (Normal, R=1.0)	Reduction Factor
1 (RH3)	SW	DCR	5.62	5.76	2.32×10^{-5}	2.16×10^{-4}	0.107
1 (RH3)	SW	TCR	5.62	5.75	3.43×10^{-6}	4.79×10^{-5}	0.072
15 (LH5)	NSW	DCR	5.63	5.76	2.35×10^{-5}	1.81×10^{-4}	0.130
15 (LH5)	NSW	TCR	5.63	5.74	3.04×10^{-6}	4.02×10^{-5}	0.072

R=0.7 across the energy scan. In this mode, the lower voltage on the entrance ESA changes the K-factor (Table 7) and shifts the FOV coverage away from the S/C (i.e., along -x in Figs. 1 and 4) to $-5°$ in elevation angle. From the azimuthal scan at the aperture boresight scan (Fig. 17), the azimuthal coverage of $\Delta\varphi \sim 6.6°$ is used to estimate G_E.

The transmission response of the CoDICE-Lo ESA in elevation angle and energy for DCRs is shown in Fig. 17. Results for position coincidence (singles), DCR, and TCR are largely consistent with each other (not shown). The angular resolution is ∼2.2° on average, and remains less than ∼2.5° up to ∼10 keV/q. The ion focusing effect due to the PAC reduces the angular resolution to ∼2.0°. The energy resolution $\boldsymbol{\sigma}_E$ was ∼6% on average. It decreases at lower energies to 5% at ∼20 keV/q and increases to ∼6.5% at 80 keV/q.

Figure 18 presents the variation of the G_E with azimuth (φ) at 4 and 16 keV/q. The figure shows that the G_E values are consistent across different azimuth locations within 50% for each type of coincidence rate, indicating uniform sensor performance and accurate assembly. Table 7 summarizes the CoDICE-Lo ESA performance for 16 keV protons by comparing the RGFO and normal geometric factor modes in two locations, namely, RH3 (rate-index 1) in the SW direction and LH5 (rate-index 15) in the NSW direction. The RGFO mode yields a reduction factor of ∼0.1 in DCR and ∼0.07 in TCR.

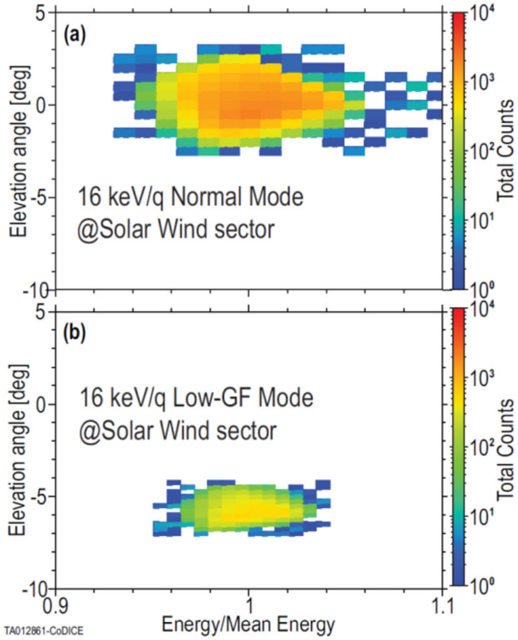

Fig. 17 Transmission responses of CoDICE-Lo instrument for a solar wind sector with normal operation mode (top) and low G-factor mode (bottom). Both figures show the DCR rates

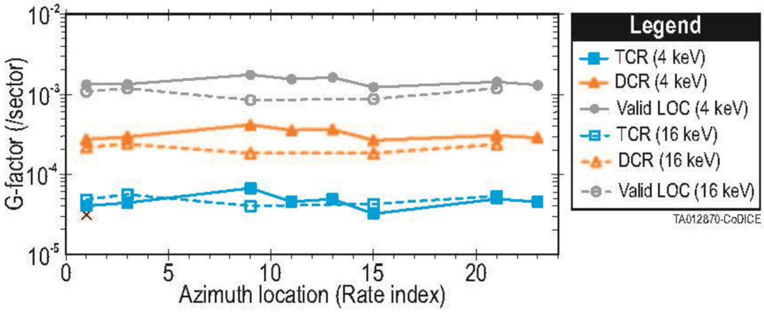

Fig. 18 Dependence of the geometric factor G_E (cm^2 str eV/eV) as a function of azimuth (Az), as determined for position coincidence rates (valid LOC, gray), double coincidence rates (DCR, orange), and triple coincidence rates (TCR, blue). Location number 1 is the solar wind sector, and the incremental number represents the azimuth location in a clockwise sense as viewed top-to-down from the sensor top cap. The geometric factor investigated using data from 8 of the 24 azimuthal sectors

5.3 CoDICE-Hi Collimator Performance

CoDICE-Hi physical geometric factor is 0.045 cm^2 sr for each of the 12 sectors as calculated from the SIMION model. Figure 19 presents the angular coverage for CoDICE-Hi for a) elevation and b) azimuth. Figure 19a shows DCR rates using a 300 keV H^+ beam at two locations using prototype apertures equipped with thin (non-flight) and thick (i.e., flight-like) foils without the ESA installed. The Gaussian-like distributions indicate consistent angular response essentially independent of the foil thicknesses. The azimuth angle scans (Fig. 19b) show the DCRs and TCRs for alphas from Thorium-228 using the full flight configuration for two adjacent apertures. Figure 19 confirms that CoDICE-Hi has reliable

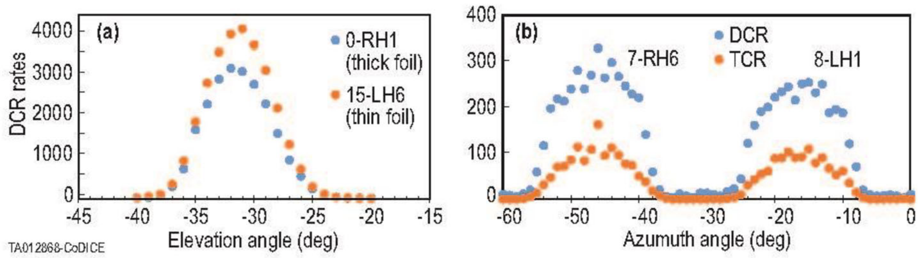

Fig. 19 a) Angular coverage for CoDICE-Hi, showing the DCR vs. the elevation angle scans in two locations using 300 keV H^+ beam. This testing was conducted using prototype apertures with thin and thick (i.e., flight-like) foils without the ESA. b) Horizontal angle scans for two adjacent apertures was conducted with the full flight configuration using the Thorium-228 radioactive source

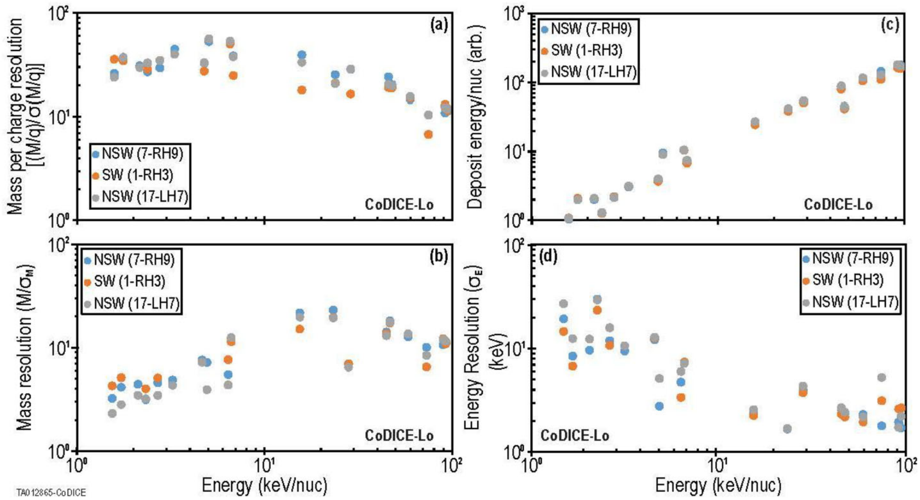

Fig. 20 a) Mass-per-charge, b) and Mass resolution for CoDICE-Lo, c) Energy Response and d) Energy resolution for APDs. These data are obtained using ion species with masses between 1–40 amu and energy between 1–80 keV/q. Data shown are for two non-solar wind (NSW) and the solar wind (SW) directions, respectively

and consistent elevation and azimuthal coverage. We also confirmed the detection efficiency, TOF performance uniformity, and the whole sky coverage using a 300 keV H^+ beam and a Thorium-228 radioactive source across all 12 apertures of CoDICE-Hi. These results confirm simulation results from the ray-tracing model that only those ions entering the two adjacent apertures create DCRs and TCRs, with essentially very few ions deviating from the gaussian-like distribution in Fig. 17b.

5.4 TOF and Energy Performance

Figure 20 summarizes the TOF and E performance for CoDICE-Lo obtained injecting ion beams of various energies between ∼1–80 keV/q and masses between 1–40 amu through the ESA followed by post-acceleration into the TOF/E subsystem for the SW sector and one representative NSW sector on each side. The mass per charge resolution shown in Fig. 20a

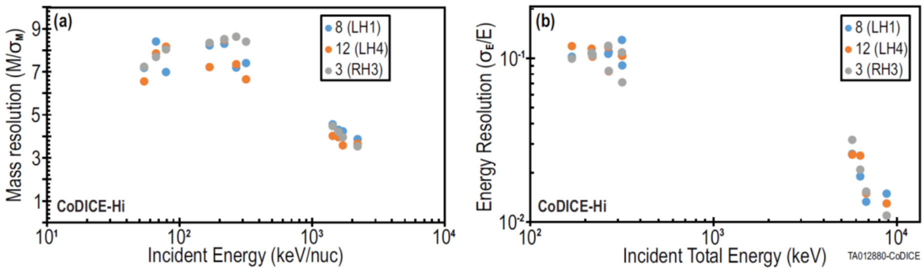

Fig. 21 a) Expected mass and b) energy resolution of CoDICE-Hi, evaluated by combining TOF and Energy measurements as a function of the incident ion's energy per nucleon. Data shown are selected for one RH side and one LH side for the non-sunward (NSW) sector, and the sunward direction (LH1). The lower energy range was evaluated using proton and Helium ion beams, and the higher energy range was evaluated using the Thorium 228 radioactive source

decreases as the E/nuc. increases, particularly above ∼10 keV/nuc, but remains above ∼10 over the entire range. This trend is consistent across different sectors (not shown). Similarly, Fig. 20b illustrates that the mass resolution ($M/\boldsymbol{\sigma}_M$) improves with increasing E/nuc. because the energy resolution of APDs improves (Fig. 20d). The energy response of the APDs, shown in Fig. 20c, exhibits a linear relationship between the incident energy and the deposited energy from ∼2 keV/nuc up to >100 keV/nuc.

Figure 20d shows the energy resolution ($\boldsymbol{\sigma}_E$) of the APDs as a function of incident energy divided by the number of nucleons of the incident ions. The incident energy includes the additional 15 keV post acceleration energy for all particles, thus the minimum energy per nucleon of the incident particles shown in Fig. 20d is mass dependent: ∼15 keV for H and ∼3.75 keV/nuc for He. The lower-energy range, i.e., below ∼4 keV/nuc, is dominated by ions heavier than He. The total energy resolution $\boldsymbol{\sigma}_E$ is plotted vs the incident energy-per-nuc and is ∼10–20 keV near the lower-energy end (for the heavier ions) improves to ∼2–3 keV near the upper-energy range. For reference, the lowest energy data shown in the plot is for 63 keV Ar which has $\boldsymbol{\sigma}_E/E \sim 0.49$. These results indicate that the APDs can accurately measure the energy of incoming particles between ∼1–100 keV/nuc, thus enabling CoDICE-Lo to differentiate between various ion masses and charge states throughout the L3 required energy range of ∼0.5–80 keV/q (Table 2). Furthermore, the alignment of the data points in NSW and SW demonstrates the uniformity of CoDICE-Lo for precise energy measurements of both the solar wind and suprathermal particle populations.

Figures 21a and 21b show the CoDICE-Hi mass and energy resolution, respectively, for the SW direction (LH1) and one representative sector on either side of the NSW sector. We used proton and helium beams <300 keV/q and a Thorium-228 radioactive source that produces alpha particles above ∼5 MeV to calibrate the high and medium gains, respectively of the SEB ASIC (Sect. 3.2.2.3). Note that the estimated mass resolution for CoDICE-Hi is plotted as $M/\boldsymbol{\sigma}_M$, while the SSD energy resolution as obtained from calibration results is shown as $\boldsymbol{\sigma}_E/E$. At lower energies between ∼10–300 keV/nuc, the expected mass resolution $M/\boldsymbol{\sigma}_M$ is ∼6–9 and is >3 above ∼2 MeV/nuc. While the energy resolution of the CoDICE-Lo APDs is determined by the ion energy loss processes in the silicon and is mass dependent, the energy resolution of the CoDICE-Hi SSDs depend only on the constant electronics noise and statistical noise ($\sim \sqrt{E}$). Our results are consistent with typical SSDs, and, as expected, the energy resolution $\boldsymbol{\sigma}_E/E \sim 0.1$ near the lower energy range (∼150 keV) improves to ∼0.01 at higher energies. Based on test pulse measurements, CoDICE-Hi is expected to measure ions from ∼0.1 to 160 MeV in total energy. This trend and performance is

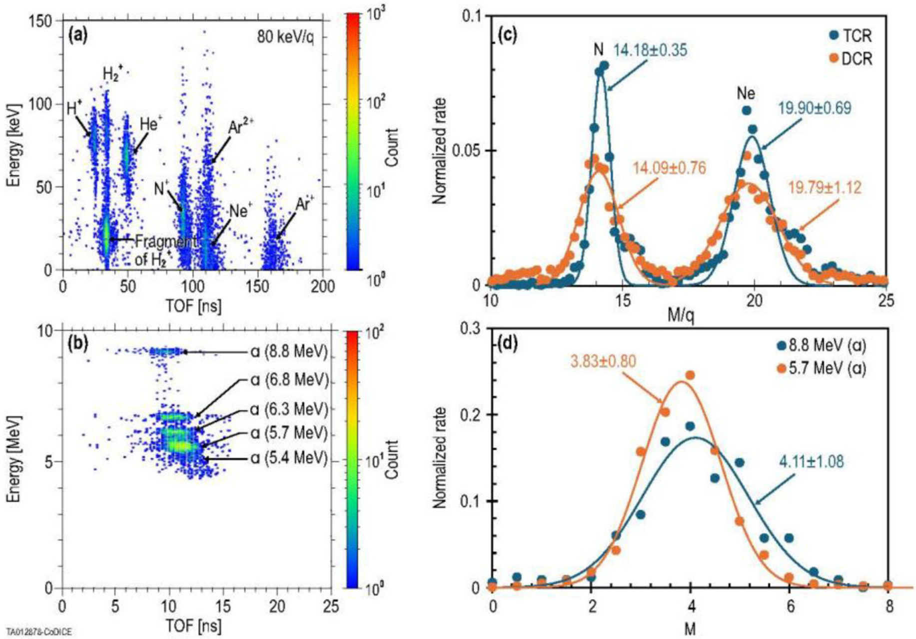

Fig. 22 a) CoDICE-Lo TOF vs E vs count for the NSW sector (17-LH7, right) for several species and energies. b) CoDICE Hi TOF vs E vs counts for multiple alpha peaks from Thorium-228. c) Mass-per-charge histograms of Ne in CoDICE-Lo; and d) Mass histogram of He in CoDICE-Hi

similar across different sectors (not shown), thus indicating reasonably consistent mass resolution irrespective of the measurement direction. Overall, Fig. 19 validates the CoDICE-Hi performance, which meets or exceeds the L3 requirements (Table 1) for resolving various ion species, especially ^{3}He and ^{4}He, over the ~0.1–>2 MeV/nuc energy range.

Figure 22a displays the counts vs TOF vs E_{Res} for several species and energies in the NSW sector (17-LH7) of CoDICE-Lo. The charge state separation capability is demonstrated by the excellent M/q (TOF) separation and in particular, the horizontal separation between Ar^+ and Ar^{2+} and the vertical separation between H_2^+ and the H, which is a fragment of H_2^+ that splits as it goes though the START carbon foil. Other species clearly identified here are H^+, He^+, N^+, and Ne^+. Figure 22b shows the TOF-E matrix for CoDICE-Hi where the multiple alpha peaks from the Thorium 228 are well resolved at the ~1–2 MeV/nuc energy range. Figures 22c and 22d show the mass-per-charge and mass histograms of Ne and He ions in CoDICE-Lo and CoDICE-Hi, respectively. Note that these data are taken near the upper energy range of both measurement systems, where the resolutions are degraded (see Figs. 20a and 21a) compared with the corresponding lower energy ranges. Thus, CoDICE-Lo can separate the isotopes of interstellar PU Ne and CoDICE-Hi can separate He isotopes (Table 1) over the desired energy ranges.

5.5 In-Flight Calibration

CoDICE in-flight calibration consists of gain checks for detectors and in-flight comparison with SWAPI and HIT. Both START and STOP MCP operational voltages will be scanned from −400 V to +100 V around their nominal values in 100 V increments. The APD/SSD bias voltages will be scanned from −40 V to +10 V around their nominal values at 10 V increments. After each test, voltages return to their nominal settings. During these tests, nominal science mode data will be collected for one 16-spin (∼4 minute) cycle at each voltage step. Therefore, the entire gain check sequence produces 24 full-cycle data from CoDICE-Hi and -Lo, which will take ∼1 hour to complete. CoDICE executes regular gain tests using an onboard Relative Times Sequence (RTS) initiated by a command per detector system from the S/C. These commands are executed at a monthly cadence initially after launch.

On board calibration comprises populating the CoDICE-Lo M vs M/q and the CoDICE-Hi Mass vs E_{Inc} matrix (Fig. 27) with real events so that the instrument response to the full range of species and energies can be characterized. These data will enable updates to the species tracks and box locations in the two matrices used by the CDH to create the rates products (see Sect. 6.5.2).

In-flight comparisons with SWAPI and HIT are performed routinely using validated data from both instruments. CoDICE-Lo provides full 3D VDF observations, while SWAPI measures full energy distributions of the core solar wind. CoDICE-Hi and HIT spectra will be compared in the overlapping energy range during large solar energetic particle (SEP) events. Instrument efficiencies will be monitored and adjusted when necessary. In-flight comparisons require no special commanding; all instruments operate in their nominal science modes, collecting simultaneous observations.

5.6 Cross Calibration

On ground cross-calibration efforts between SWAPI and CoDICE, and HIT and CoDICE were successful and conducted to understand the instrument responses in overlapping energy ranges. SWAPI and CoDICE were cross calibrated using the same ion beams at the Space Physics Laboratory at Princeton (see Rankin et al. 2025 for details on the facility). The cross calibration effort focused on characterizing the energy and angular responses for 2 keV/q He^+ ions and 16 keV/q He^+ ions. Both instruments were mounted in the same vacuum chamber at the same time during these tests. An absolute beam monitor (ABM) was used to measure the incident beam flux before and after each test, which was then used to normalize the instrument count rates.

Figure 23 compares the elevation angular responses of SWAPI and CoDICE obtained over 0.1° resolution by setting the ESA voltages to cover the corresponding beam energies. Both instruments exhibit broader but overlapping angular coverage with centroids near 0° in their respective normal GF modes. As expected, the CoDICE angular response in the RGFO mode is shifted relative to both the CoDICE normal mode (see Sect. 5.2, Table 7, and Fig. 17) and the SWAPI angular response. Notably, the difference in SWAPI's count rates between 16 keV and 2 keV He^+ is consistent with the $\sim 1000\times$ attenuation through sunglasses (Fig. 1b), and the CoDICE count rates during the RGFO mode are reduced by about a factor of ∼3 compared with the normal mode.

Table 8 summarizes the derived centroid energies from the ESA voltage scans at the center of the FoVs, i.e., at elevation angle of 0° for SWAPI and CoDICE normal mode, and 6° for CoDICE RGFO mode. The results for the derived centroid energies are in excellent agreement between CoDICE and SWAPI. Further analysis and in-flight data will enable us to evaluate the energy and mass-dependent efficiencies for both instruments.

CoDICE and HIT were cross calibrated using the same type (Thorium 228) of radioactive sources for α-particles in their overlapping energy range exposed to one look direction from each instrument. The Thorium sources were characterized during each test using the same,

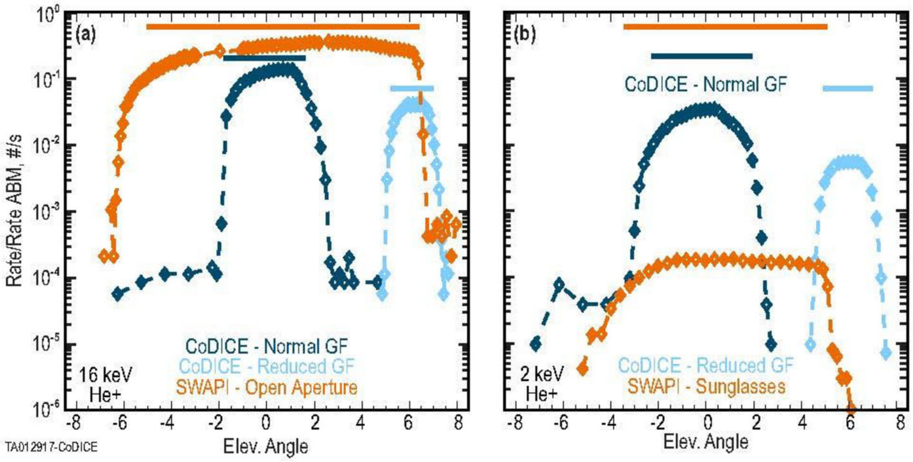

Fig. 23 Angular responses of CoDICE and SWAPI for (a) 16 keV/q He^+ and (b) 2 keV/q He^+. Orange: SWAPI; dark blue: CoDICE normal mode; light blue: CoDICE RGFO. The FHWM of the angular coverage for SWAPI and CoDICE are shown as horizontal bars

Table 8 Centroid energies derived from the ESA voltage scans for SWAPI and for CoDICE in both normal and RGFO modes. Calibrated k-factors are used to calculate the centroid energies

Energy/Species	Centroid Energy (eV/q)	
	2 keV/q He^+	16 keV/q He^+
SWAPI	1964.6	16,044
CoDICE – Normal GF	1966.1	16,099
CoDICE – RGFO	1945.7	16,020

fully calibrated "gold standard" detector and GSE, and the calibrated Thorium sources were used for instrument calibrations for HIT (Christian et al. 2026) and CoDICE (Table 5 in Sect. 5.1). The results for CoDICE-Hi are shown in Fig. 22b and similar results with alpha peaks between ∼5–10 MeV were also obtained by HIT (see Christian et al. 2026).

6 Sensor Operations

6.1 Software Overview

The CoDICE Flight Software (FSW) comprises two separate embedded applications: Boot FSW, stored in Programmable Read Only Memory (PROM), and Application (App) FSW, stored in Magnetoresistive Random Access Memory (MRAM). The PROM is not writeable in flight, so the Boot FSW is frozen, while the MRAM is writeable, and so the App FSW can be updated.

When CoDICE is powered on, the Boot FSW executes to initialize the hardware and validate stored App FSW images. Once a valid App FSW image is identified, the Boot FSW loads and runs the App FSW. The App FSW is the primary science and engineering operational software. The App FSW is responsible for processing commands, generating telemetry, monitoring instrument health and safety, controlling HVPS, and collecting science data.

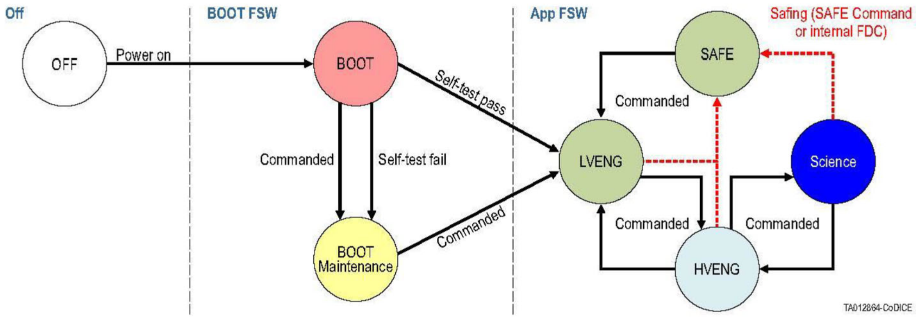

Fig. 24 CoDICE Software Modes and Transitions

Table 9 CoDICE FSW Operating Modes

Mode	Description
Boot	Indicates that the Boot FSW is running and is working to initialize hardware and bootstrap the App FSW.
Boot Maintenance	Boot FSW failsafe mode if any hardware self-tests fail or if a valid App FSW image is not found. Boot FSW remains in this mode until commanded to do otherwise. Monitor mode provides basic low-level commanding functions and the ability to upload memory.
SAFE	SAFE mode is entered upon execution of the *CMD: COD_SAFE* command or an internal Fault Detection & Correction (FDC) trigger with action set to Soft Safe. The command can be used in FDC response macros. On entry to SAFE mode, all HVPS are ramped down per the HVPS Control table in the Engineering LUT. Once all HVPS are ramped to 0 they are disabled. RTS and HVPS commands are not allowed in LVENG mode.
LVENG	LVENG (Low-Voltage Engineering) mode is the initial mode entered upon App FSW startup. All HVPS are disabled, and HVPS commands are not allowed. Most other commands are allowed.
HVENG	HVENG (High-Voltage Engineering) mode is used to enable and configure the HVPS, and for manual commanding of the HVPS during testing, calibration, and commissioning operations.
Science	FSW sweeps the ESA HVPS according to onboard configuration tables and generates science data products. The sweeping/acquisition will operate continuously until commanded out of Science mode.

6.2 Operational Modes

The Boot and App FSW implement the modes of operation described in Table 9 and Fig. 24.

6.3 Startup and Configuration

During instrument start-up, the FSW applies default settings to each of the FEE FPGAs and the four ASICs from a configuration table stored in the instrument's non-volatile memory. These default values include settings such as data rates, calibration constants, detector thresholds, gain stage saturation thresholds, and timing configurations that were selected and tuned during instrument Integration and Test (I&T).

After the instrument startup is complete, a single on-board RTS configures the instrument to its science acquisition mode. The RTS internally issues commands to enable and ramp

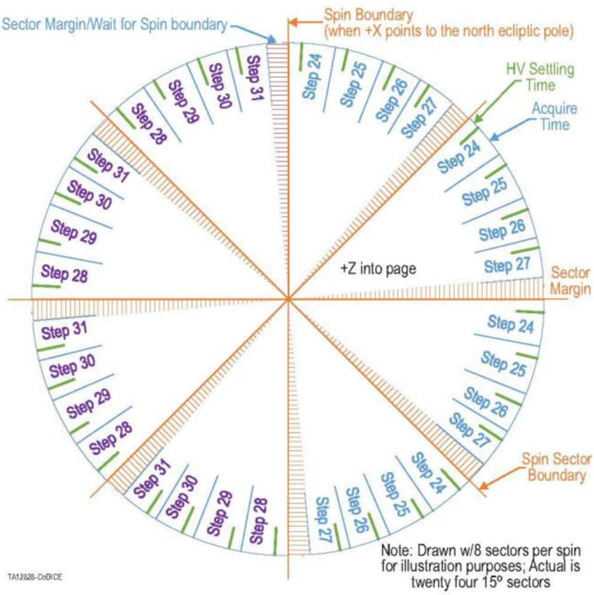

Fig. 25 Subset of ESA voltage steps acquired during one half-spin

all necessary HVPSs to operational values, configure telemetry data rates, and transition to Science mode.

6.4 Data Acquisition

6.4.1 Spin Synchronization

While in Science mode data acquisition is synchronized to the S/C spin, and each spin is subdivided into twenty-four 15° sectors. A full collection cycle occurs over 16 spins. CoDICE-Hi and CoDICE-Lo use the same spin synchronization and subdivision to have a common base for data collection and processing.

6.4.2 CoDICE-Lo

The instrument autonomously steps through 128 ESA voltages and selects ions within a range of E/q values to acquire data across the full energy range at each of the spin sectors. Due to the geometry of the instrument, a half-spin is sufficient to achieve a 360° view for a given energy step since a given detector will sweep through 0°–180° while it's opposite sweeps through 180°–360°. At the beginning of each half-spin, a subset of ESA voltages is selected, and those voltages are stepped through in each of the 12 sectors in the half spin. Over the course of 16 spins (approximately 4 minutes) CoDICE samples each of the ESA steps at each of the 15° spin-angle sectors (Fig. 25).

In the RGFO mode (see Sect. 5.2), if a second pre-defined count rate threshold is crossed, the instrument will cease sweeping to lower ESA voltages, set the ESA to a high-energy step value, and stop acquiring data for the remainder of the 16-spin cycle. This mode is referred to as No Scan Operation (NSO). The point at which RGFO and NSO are applied is reported in the Science Telemetry so that ground processing can account for the change in gain factor.

6.4.3 CoDICE-Hi

CoDICE-Hi does not include a voltage sweep, so a single acquisition is collected in each sector.

6.4.4 Periodic Adjustments

Performance of the CoDICE electronics and detectors varies with temperature, so in addition to the primary science data collection activity, the instrument performs the following adjustments at the beginning of each 16-spin cycle to maintain consistent measurements:

- TDC calibration: an FPGA calibration routine is executed to tune the ring oscillators used to convert TOF and Position data to digital values.
- APD Bias temperature compensation: AEB temperature sensors are used to inform adjustments to the APD Bias and APD Bias 2 HVPS outputs to maintain a constant gain factor for the APD detectors.

6.5 On-Board Processing

The CDH FPGA receives the three types of PHA events listed in Table 4 from the FEE FPGA with the information and metadata provided in Figs. 26a and 26b for CoDICE-Lo and CoDICE-Hi, respectively. The CDH adds appropriate metadata (energy step, spin angle, spin number) and indexes the TCR and DCR events into a series of tables. The CDH ultimately assigns a Priority and Species value to the event from CoDICE-Lo and a Priority and Species/Energy value to the event from CoDICE-Hi. Table 10 provides detailed information about these priorities and Fig. 27 show their locations in a) the M vs M/q matrix space for CoDICE-Lo and b) the Mass vs incident energy (E_{Inc}) space for CoDICE-Hi. Algorithms for estimating the M, M/q, and E_{Inc} from the PHA data are described in Sect. 7.2.

For CoDICE-Lo, priorities assign a general category for the event and cover the full M vs M/q matrix space (Fig. 27a), while species assignments provide a specific species determination, but cover only a portion of the M vs M/q matrix space. All events that fall within the regions determined by the M and M/q boundaries are counted. Ground algorithms are used to correct for overlap, when the distribution for one species falls into more than one matrix bin. For CoDICE-Hi, the priorities assign a general category for the event and cover the full M vs E_{Inc} space (Fig. 27b), while species/energy assignments provide a specific species and energy determination, but cover only a portion of the M vs E_{Inc} space. In both cases, there are 'void' spaces in the corresponding tables and matrices where an event is assigned an 'unknown' species.

6.5.1 PHA Events

Each ion that generates a TCR – a PHA or direct event is transmitted to the CDH FPGA which adds information about the event's priority and spin, as well as the energy step in case of CoDICE-Lo. This information is formatted as shown in Table 11. The raw PHA events provide full measurement details of each event, but only a sample of the collected events are selected for downlink due to bandwidth constraints. The direct event data products are produced at a cadence of 4 min for both Lo and Hi. In the nominal configuration, up to 5000 ion events for Hi and 5760 events for Lo are recorded into the L0 data packet within each 4-min accumulation period. The L1A Priority Counts data product is used to normalize the count rates and intensities derived from the Direct Event data products. The L1A Direct Events contain the bit values for each parameter, which is converted to physical units in the L2 product using calibration data.

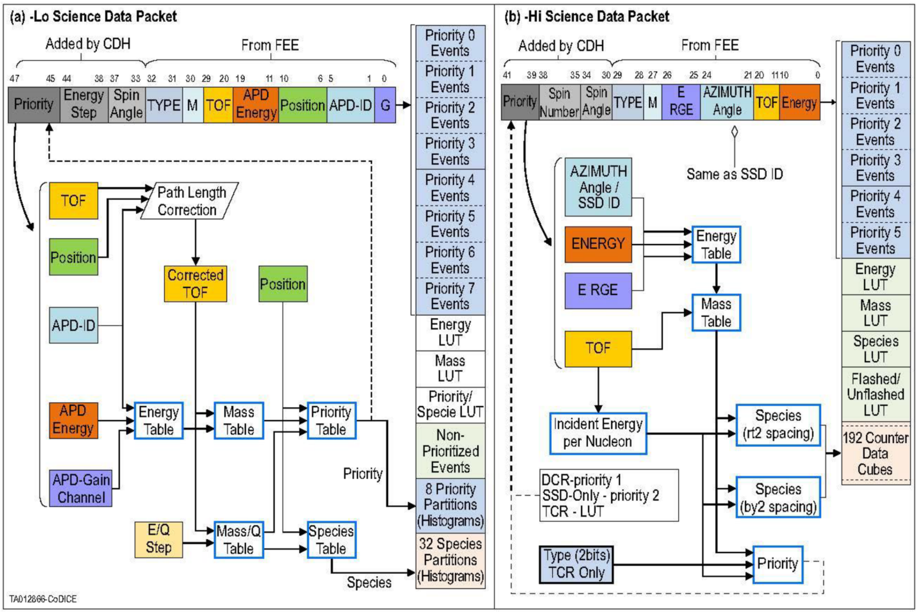

Fig. 26 CoDICE Priority and Species Assignments

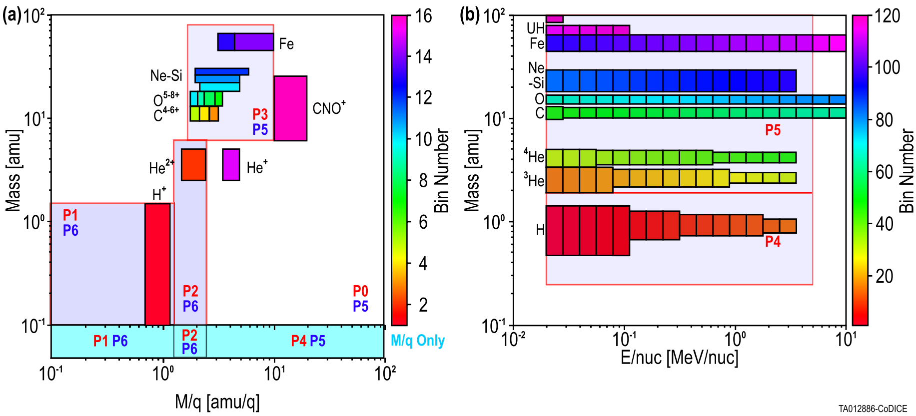

Fig. 27 a) M vs. M/q matrix for CoDICE-Lo and b) M vs. E_{Inc} matrix for CoDICE-Hi showing priorities for selecting and transmitting PHA events to the SDC. Binned data products are created by aggregating counts in pre-defined bins stored in configurable look-up-tables (LUTs) in the CDH FPGA. Examples shown here are for a) "Lo SW Species Counts" and b) "Hi Omni-directional counts"

6.5.2 Binned Data

In addition to creating and storing the PHA or direct event data in memory, the CDH/FPGA updates histograms corresponding to the various data products listed in Table 13 and Fig. 27. Figure 27 shows pre-defined bins for a) species counts for CoDICE-Lo and b) omnidirectional counts for CoDICE-Hi (Table 13). These histograms provide a more complete accounting of events, but do not provide the measurement specifics. The full set of science

Table 10 CoDICE Science Rates created by the CDH and transmitted to ground

CoDICE-Lo		CoDICE-Hi	
Priorities		*Priorities*	
P0	SW Triple Coincidence PUIs	P0	No Triple Coincidence
P1	SW Sector H^+	P1	Double Coincidence
P2	SW Sector He^{++}	P2	SSD
P3	SW Sector High Charge State Heavies	P3	Unused
P4	SW Sector Double Coincidence PUIs	P4	H
P5	NSW Sector Heavies	P5	Heavies
P6	NSW H^+ and He^{++}		
P7	Unused		
Species		*Omni Species*	
*S1	SW – H^+	S0 – S43	Unused
*S2	SW - He^{++}	S44	junk
S3	SW - C^{4+}	S45 – S59	H for different energy bins
S4	SW - C^{5+}	S60 – S74	^{3}He for different energy bins
S5	SW - C^{6+}	S75 – S89	^{3}He for different energy bins
S6	SW - O^{5+}	S90 – S107	C for different energy bins
*S7	SW - O^{6+}	S108 – S125	O for different energy bins
S8	SW - O^{7+}	S126 – S140	Ne + Mg + Si for different energy bins
S9	SW - O^{8+}	S141 – S158	Fe for different energy bins
S10	SW - Ne	S159 – S163	UH for different energy bins
S11	SW - Mg	S164	junk
S12	SW - Si	*Sectored Species*	
*S13	SW - Fe lowQ	S165	junk
S14	SW - Fe highQ	S166 – S173	H for different energy bins
S15	SW - He^+ (PUI)	S174 – S181	^{3}He, ^{4}He for different energy bins
S16	SW - CNO^+ (PUI)	S182 – S189	CNO for different energy bins
S17	NSW - H^+	S190 – S197	Fe for different energy bins
*S18	NSW - He^{++}		
S19	NSW - C		
S20	NSW - O		
S21	NSW – Ne + Si + Mg		
S22	NSW - Fe		
S23	NSW - He^+		
S24	NSW - CNO^+		
S25-S32	Unused		

*Used for angular intensity data products

rates in each raw data packet that is telemetered to the S/C and then transferred to the SDC is also listed in Table 11.

6.6 Telemetry

CoDICE telemetry is grouped into seven categories listed below and in Table 12.

Table 11 CoDICE Direct Event Bit Allocations

CoDICE Hi (42-bits)		CoDICE-Lo (48 bits)	
Number of Bits	Description	Number of Bits	Description
11	SSD Energy	1	APD Gain
10	TOF	5	APD ID
4	SSD ID	5	Position
2	Energy Range (Gain)	9	APD Energy
1	Multi-Flag	10	TOF
2	PHA Type	1	Multi-Flag
5	Spin Sector (0–23)	2	PHA Type
4	Spin Number	5	Spin Sector
3	Priority	7	ESA Step
22	Spare	3	Priority
		16	Spare

1. ICD: Autonomy packet required per the Spacecraft ICD
2. Boot: Packets generated by the Boot FSW
3. Engineering: Packets that provide an overview of the instrument's health and status
4. Diagnostic: Packets that provide detailed internal information, such as hardware register dumps and software state. These packets are large and provide a lot of redundant information and so are typically disabled except when being used during real-time testing and diagnostics operations.
5. Lo Science: CoDICE-Lo science data
6. Hi Science: CoDICE-Hi science data
7. I-ALiRT: CoDICE Real-time data

Except for Memory Dump packets, all ICD, Boot, Engineering, and Diagnostic packets are fixed length, and none of the packets in these categories are compressed. Lo Science and Hi Science packets are variable length due to dependence on the number of received events and compression.

6.7 Data Compression

Both the Hi Science and Lo Science packets are compressed. CoDICE implements two table-based 24-to-8 bit Lossy compression algorithms (referred to as Compression A and Compression B) and a lossless LZMA compression. An additional compression method, Pack 24-bit, packs count values into 24-bit fields where the values do not exceed 24-bits, thus avoiding transmission of redundant zero-bits to the ground. Table 12 also shows the compression configuration for each of the Science data products.

6.7.1 Lossy Compression

Lossy compression is applied to counts data products as the first stage compression to reduce data volume. Lossy compression is roughly log-based, with exceptions at the low end for greater precision, and at the high end for greater range. Lossy compressions A and B are identical for the lower 75% of the compressed-value range, then compression B deviates to provide a higher range for singles counters that can reach very large values when aggregated.

Table 12 CoDICE Telemetry

Category	Packets	Compression	Downlink bps (Science Mode)
ICD	Autonomy	None	0
Boot	Boot HK, Boot Memory Dump	None	0
Engineering	Nominal HK, Event Messages, Memory Dump, Static HK, RTS status	None	45
Diagnostic	CDH, Sensor HV, Optics HV, APD FEE, SSD FEE, FSW, System Variables	None	0
Lo Science	Raw PHA Events; Solar Wind Priority Counts, Species Counts, Angular Counts; Non-Solar Wind Priority Counts, Species Counts, Angular Counts; Aggregated Instrument Counters; Singles Instrument Counters;	Lossless (Raw PHA) Lossy A + Lossless (Species/Priority Counts) Lossy B + Lossless (Instrument Counts)	2381 (assumes 2:1 lossless compression)
Hi Science	Raw PHA Events, Priority Instrument Counters, Omnidirectional Species Counts, Sectored Species Counts, Aggregated Instrument Counters, Singles Instrument Counters	Lossless (Raw PHA) Lossy A + Lossless (Species/Priority Counts) Lossy B + Lossless (Instrument Counts)	753 (assumes 2:1 lossless compression)
I-ALiRT	Lo, Hi Real-time Space Weather	Pack 24-bit (Lo); Lossy A (Hi)	336

6.7.2 Lossless Compression

Lossless LZMA compression is applied to all Science data products except for Hi and Lo I-ALiRT. For the data products that are subject to Lossy compression, this Lossless compression is applied as a second stage.

7 Data Products and Algorithms

CoDICE transmits two types of L0 data products to the SDC: direct or PHA events and onboard processed or binned data products (Fig. 28, Tables 11, 13). Figure 28 describes how the L0 data are processed to produce the L1-L3 higher level data products summarized in Table 12. These are: Level 0–the raw CCSDS packets, Level 1a: Raw count data decommutated into formatted variables; Level 1b – Counts converted to count rates; Level 2–Validated data products with count rates converted to intensities using instrument calibration factors; Level 3–Higher level products. The direct event data products contain the complete measurement information for each ion event that is telemetered based on the priority schemes, while the binned data provides counts (L1a), count rates (L1b), and intensities (L2) as a function of energy, polar angle, and spin angle at different cadences depending on the data product.

CoDICE-Lo counts (L1a), count rates (L1b), and intensities (L2) are sorted into two broad angular ranges, namely: 1) the SW or sunward direction covers a 75-degree cone centered on the spacecraft spin axis which includes 5 azimuths, and 2) the NSW direction covers the remaining 19 azimuths. These two data products are provided as 1D and 3D VDFs for multiple species. CoDICE-Hi provides the intensities of ∼0.03–5 MeV/nuc. suprathermal

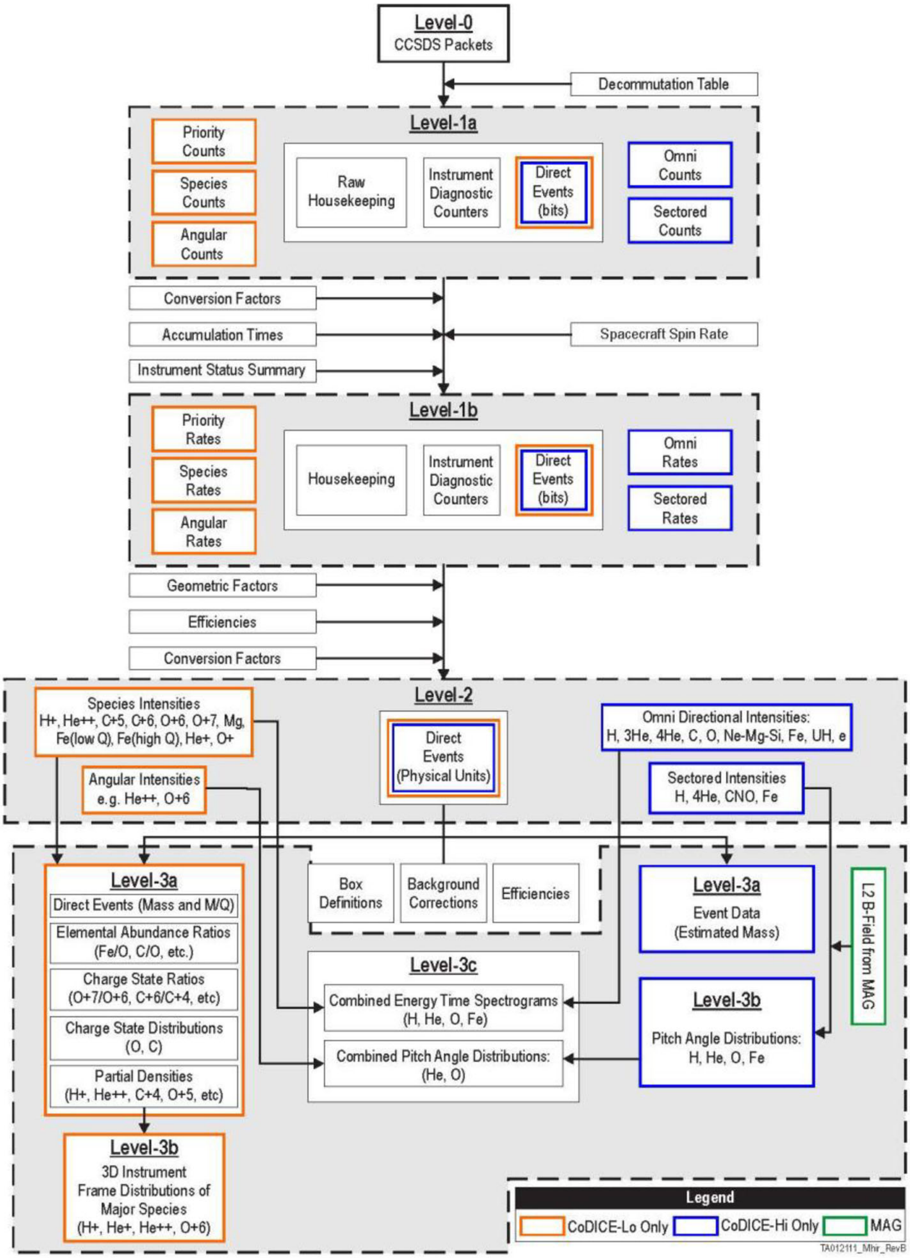

Fig. 28 Pipeline of CoDICE data products from L0-L3 available at the IMAP SDC

through energetic H-Fe ions in 12 azimuthal sectors and 12 spin angles. L2 angular data products are provided in the S/C frame. CoDICE data products and algorithms in the data production pipeline at the SDC are validated through point-by-point comparison to products produced independently using known input and output datasets.

Table 13 CoDICE L1 – L3 data products

	Common	CoDICE-Lo	CoDICE-Hi
Level 1 a/b	Instrument Counters – APD/SSD and MCP counts/rates. Housekeeping – Instrument voltages, currents, and digital settings. Direct Events – (see Table 9).	Species counts/rates: SW/NSW counts/rates of H–Fe for 128 ESA steps. Angular counts/rates: SW counts/rates for H^+, He^{2+}, O^{6+}, and Fe (low charge state) and NSW counts/rates for He^{2+} in 24 spin sector × 24 position bins for 128 ESA steps. Priority counts/rates: Counts/rates in 24 spin sector bins for 128 ESA steps. SW Priorities: P0-TCR, P1-H^+, P2-He^{2+}, P3-HeavyIons, P4-DCR. NSW Priorities: P5-HeavyIons, P6-H^+-He^{2+} (see Fig. 25, top).	Omni-Directional counts/rates for H–Fe (Fig. 25), summed over all SSDs and spin sectors and binned into energy-per-nuc bins with logarithmic spacing of sqrt(2) Sectored counts/rates for H, 3He, 4He, C+N+O, and Fe in 12 spin sectors for 12 azimuths (SSD ID), binned into energy-per-nuc bins with logarithmic spacing of 2. Priority counts/rates for each priority. P0-NoTCR, P1-DCR, P2-SSD, P3-N/A, P4-H, P5-HeavyIons.
Level 2	Direct Events – Event data converted to physical units: spin angle, elevation angle, Energy (MeV), TOF (ns), E/q (Lo), and E/n (Hi).	Species Intensities: SW/NSW intensities of 0.5–80 keV/q H–Fe in 128 E/q steps at 4 min cadence. Angular Intensities*: SW/NSW intensities of 0.5–80 keV/q in 128 E/q steps × 3 in SW and 10 in NSW polar angles × 24 spin angles bins at 4-min cadence.	Omni-Directional Intensities: for 0.05–2 MeV/nuc H–Fe at 1-min cadence Sectored Intensities*: for 0.05–2 MeV/nuc H-Fe in 8 energy bins × 12 polar angles × 12 spin angles at 4-min cadence.
Level 3a	Direct Events – All PHA event data from L2 products with additional estimates of Mass (Hi & Lo) and M/q (Lo).	Partial Density of SW Species – Derived from L2 species intensities. Elemental Abundances+: C/O, Mg/O, Fe/O at 12-min cadence. Ionization Charge State Ratios & Distributions+: C^{6+}/C^{5+}, C^{6+}/C^{4+}, O^{7+}/O^{6+}, Fe_low/Fe_high. Distributions: O^{5+}-O^{6+}, C^{4+}-C^{6+} at 12-min cadence.	N/A
Level 3b	N/A	3D Velocity Distribution Functions (VDFs)*: for H^+, He^+, He^{2+}, and O^{6+} in 128 E/q steps × 13 polar angles × 24 spin angles at 4-min cadence.	Pitch Angle Distributions*: Intensities of H, He, CNO, and Fe as a function of pitch angle in 8 E/nuc bins × 6 pitch angle bins at 4-min cadence.
Level 3c	Combined Pitch-angle Distributions and Energy-time spectrograms for H, He, O, and Fe		

*Provided in the S/C frame. +Derived from CoDICE-Lo L3a Partial Density data product.

7.1 L0 to L1 Data Processing

The L0 data packets are provided as a series of spin-sector × spin number data cubes (or counters) collapsed per the onboard science lookup table (SCI_LUT). The collapsed data cubes are also optionally compressed using Lossy and/or Lossless Compression. As part of the L0 to L1A data processing, the compressed data cubes are decommutated based on the SCI_LUT spreadsheet into data arrays with dimensions depending on the specific data product. For example, the data array for CoDICE-Lo L1A SW/NSW Angular Counts has dimensions 128 E/q steps × 5/19 positions × 12 spin sectors.

Table 14 Key quantities used to create L1-L3 data products at the IMAP SDC

Common	R_j	Count Rate for species j	#/s
	J_j	Differential intensity for species j	Lo: # / (cm^2 s sr keV/q)Hi: # / (cm^2 s sr MeV/nuc)
Lo	G_E	Energy Geometric Factor – dependent on SW/NSW sector and operation mode, RGFO or Normal (Table 7)	cm^2 sr eV/eV
	ε_{jlk}	Efficiency for species j, ESA step l, and rate index k (Table 6)	unitless
	$(E/q)_l$	Energy per charge passband of ESA step l	keV/q
	Indices	j = species, l = ESA step (1–128), k = rate index (1–24), n = spin sector index (1–24)	
Hi	G_k	Physical GF for a single SSD	cm^2 sr
	ε_{jik}	Efficiency for species j, energy-per-nuc bin i, and rate index k	unitless
	ΔE_{ji}	Energy-per-nuc pass band for species j, energy-per-nuc bin i	MeV/nuc
	Indices	j = species, i = energy-per-nuc bin index (number depends on product), k = rate index (0–15), n = spin sector index (1–12)	

Due to the non-uniform ESA stepping scheme of CoDICE-Lo FOV which occurs over 32 half-spins of the spacecraft, a given position and ESA step will only sample 180° in spin angle. Thus, the reported spin sector in the L0 data maps to different physical spin angles depending on the ESA step and position sample. To account for this, the L1A SW/NSW Angular Counts are reformatted into count arrays which consists of counts as a function of 128 ESA Steps × 5/19 azimuth angles × 24 spin angle sectors, where the spin angle sector corresponds to the physical spin angle sampled over 360°. This de-spinning algorithm is also applied to the Direct Event data products when converting from L1A to L2.

For both CoDICE-Hi and CoDICE-Lo the L1B data products are computed by dividing the L1A counts by the flight software acquisition time, which depends on each respective data product. The total accumulation time for each data product is computed based on the nominal acquisition time corresponding to a single 15° spin sector ($t_{acquire}$)for each ESA step (in the case of CoDICE-Lo), as well as the number of position/SSDs and spin sectors over which the data product is accumulated. For example, the Hi omni-directional counts are summed over 24 spin sectors and 4 spin periods. Thus, the acquisition time used to convert to count rates is given by: $24 \cdot 4 \cdot t_{acquire}$.

7.2 L1 to L2 Data Processing

Table 14 lists the key quantities used to create the L1-L3 data products.

7.2.1 CoDICE-Lo

Solar Wind Species, SW Intensities For the beam-like solar wind species we calculate the intensities assuming a distribution centered on azimuth 0° (rate index 1 in Table 6), i.e., the position viewing along the spin axis. We use G_E to convert the L1B Species Rates, $R_j(l)$, to intensity, $J_j(l)$, as follows:

$$J_j(l) = \frac{R_j(l)}{G_E \cdot \varepsilon_{jl1} \cdot (E/Q)_l} \tag{5}$$

G_E ("Normal" or "RGFO") is determined by checking whether the half-spin number for the ESA step l is less than the half-spin number specified by the parameter RGFO_Half_Spin. If the half-spin is less than RGFO_Half_Spin, then the "Full" geometric factor is used. If it is greater than or equal to RGFO_Half_Spin, then the reduced geometric factor is used.

Pick-up Ion Species, SW and NSW Intensities For PUI species rates for He^+, O^+, and Ne^+, we assume isotropic distributions over N=5 azimuths for the SW (rate indices 1, 2, 3, 23, 24 in Table 5) and over the remaining N=19 azimuths for the NSW directions and calculate the corresponding intensities using:

$$J_j(l) = \frac{\mathrm{R_j}(l)}{N \cdot G_E \bullet \varepsilon_{jl} \bullet (E/Q)_l} \tag{6}$$

Angular Intensities The CoDICE-Lo L2 angular intensities are provided as differential intensity for a set of species sorted by energy-per-charge, azimuthal and spin angles, and calculated from the L1B Angular rates $\mathrm{R_j}(l, k, n)$ arrays using:

$$J_j(l, k, n) = \frac{\mathrm{R_j}(l, k, n)}{G_E \bullet \varepsilon_{jlk} \bullet (E/Q)_l} \tag{7}$$

7.2.2 CoDICE- Hi

Omni-Directional Intensities The omni-directional intensities are computed from the L1B omni-directional rates which are provided as a function of energy-per-nuc for select ion species using:

$$J_j(i) = \frac{R_j(i)}{\left(\sum_k G_k\right) \cdot \left(\frac{\sum_k \epsilon_{jik}}{12}\right) \cdot \Delta E_{ji}} \tag{8}$$

Sectored Intensities CoDICE-Hi L2 sectored intensities for each species (j) as a function of energy bin (i), SSD ID (k), and spin sector (n) are calculated from the L1B Sectored Count Rates product using:

$$J_j(i, k, n) = \frac{R_j(i, k, n)}{G_k \cdot \epsilon_{jik} \cdot \Delta E_{ji}} \tag{9}$$

7.3 L2 to L3 Data Processing

7.3.1 L3a PHA Event Data

L3 Direct event data products are derived by converting the L2 PHA direct events from instrument units (TOF in ns; E_{Res} in MeV or keV) to physical units of M and M/q for CoDICE-Lo and Mass and E_{Inc} for CoDICE-Hi.

1. CoDICE-Lo

Mass and M/q The CoDICE-Lo event data contains estimates of the particle mass and mass-per-charge which are determined using an empirical formula. The mass-per-charge of each event is given by:

$$M/q = 2 \cdot (E/q + PAC - \alpha) \cdot (\tau/d)^2 = (E/q + PAC - \alpha) \cdot \tau^2 \cdot K \tag{10}$$

Here, E/q is the energy-per-charge, based on the ESA step (in keV/q), PAC is the post-acceleration voltage (default 15 kV, constant), α is an approximation for energy losses in the carbon foil, τ is the TOF (ns), d is the path length ∼10.64 cm, K is a conversion factor to account for different units and constants included in the calculation, given by:

$$K = 1.692 \times x10^{-5}\text{amu}\left(\text{keV} \cdot \text{ns}^2\right)^{-1} \tag{11}$$

The mass of each event is estimated using a polynomial function of the logarithm of the event energy (E_{Res}) and time-of-flight (τ). With X = ln(E_{Res}) and Y = ln(τ), we first compute Z as:

$$Z = A_0 + A_1X + A_2Y + A_3XY + A_4X^2 + A_5Y^3 \tag{12}$$

Here, A_i are coefficients determined from analysis of calibration data. The final particle mass in amu is given by:

$$M = e^Z \tag{13}$$

2. CoDICE-Hi

Mass and E_{Inc} The mass M of each CoDICE-Hi PHA event is estimated using E_{res} and TOF (τ), and the incident energy E_{Inc} is estimated from the energy-per-nuc calculated from the TOF measurements after accounting for energy losses through the Hi collimator foils and the START foils. The E_{inc} is also validated using the E_{res} after accounting for energy losses through the Hi collimator foils and START foils, the SSD dead layer, and pulse height defect in the SSD (Galvin 1982):

$$M \sim E_{\text{SSD}} \cdot f\left(\tau_{ch}\right) \tag{14}$$

where τ_{ch} is the TDC channel number (Sect. 3.2.3.1) and:

$$f\left(\tau_{ch}\right) = \left(a_0 + a_1\tau_{ch} + a_2\tau_{ch}^2\right)^2 \tag{15}$$

is determined from on-ground calibration and analysis. Finally, the incident energy is given by:

$$E_{\text{Inc}} = \varepsilon_1 \cdot E\left(\text{TOF}\right) = \varepsilon_2 \cdot E_{\text{SSD}} \tag{16}$$

where ε_1 and ε_2 depend on the species, energy, ASIC charge-division gain channel, and SSD ID.

7.3.2 L3a and L3b

CoDICE-Lo L3a partial densities are derived from the L2 Species Intensities product from the SW direction for each individual charge state. These partial densities are then used to compute L3b elemental abundance ratios (Fe/O, Mg/O, C/O) and charge state ratios (C^{6+}/C^{5+}, C^{6+}/C^{++}, O^{7+}/O^{6+}, and Fe(low q)/Fe(high q), as well as charge state distributions for O and C.

CoDICE-Lo L3b 3D Instrument Frame Distributions are computed from the L3a Event Data. The event data is first binned into a 3D count array, which is then converted to intensities after applying normalization factors derived from the L1A Priority Counts. The final product consists of intensities as a function of polar angle, spin angle, and energy-per-charge for major species H^+, He^+, He^{++}, and O^{6+}.

CoDICE-Hi L3B Pitch Angle Distributions are computed for He and O from the L2 Sectored Intensities and the magnetic field vector averaged over the Hi measurement time period. The final product contains intensities as a function of energy and pitch angle at 4-min cadence.

7.4 Combined CoDICE-Lo and CoDICE-Hi Data Products

L3c. Combined Energy-Time Spectrograms This product consists of intensities of major species H, He, O, and Fe covering the full CoDICE energy range at 4-min cadence. Level 2 data products are used to produce a single combined energy-time spectrogram for each species. The first step is to produce energy-time spectrograms from Lo and Hi for each species in a common format.

Step 1: Convert CoDICE-Lo Distributions to E/nuc

We use SW and NSW data from the L2 Species Intensities product. For each species, j, the intensities $(J_j(l))$ are provided as a function of 128 energy-per-charge values (indexed by l). Since the L2 data is provided as a function of energy-per-charge, we perform the following steps for each species to convert the units to energy-per-nuc in units of MeV/nuc. The converted Lo intensities and energy bins are referred to as $\tilde{J}_j\,(l)$ and $\tilde{E}_H$.

Hydrogen: With Q=1, M=1 amu, the converted Lo Hydrogen product is given by:

$$\tilde{J}_H\,(l) = \frac{\left(J_{H,\mathrm{SW}}\,(l) + J_{H,\mathrm{NSW}}\,(l)\right)}{Q} \cdot M \cdot 1000 \tag{17}$$

$$\tilde{E}_H = \frac{E_H}{M \cdot 1000} \tag{18}$$

$J_{H,\mathrm{SW}}\,(l)$ and $J_{H,\mathrm{NSW}}\,(l)$ are the SW and NSW H intensities from the L2 Species product, and the factor of 1000 converts keV to MeV.

Helium: With charge q=2 and M=4, the converted Lo He^{2+} product is computed as:

$$\tilde{J}_{\mathrm{He}}\,(l) = \frac{\left(J_{\mathrm{He}^{2+},\mathrm{SW}}\,(l) + J_{\mathrm{He}^{2+},\mathrm{NSW}}\,(l)\right)}{q} \cdot M \cdot 1000 \tag{19}$$

$$\tilde{E}_{\mathrm{He}} = \frac{E_{\mathrm{He}} \cdot q}{M \cdot 1000} \tag{20}$$

Oxygen: Since Lo measures four different charge states of Oxygen, we convert each of the individual charge state distributions to common units by:

$$\tilde{J}_{O,q}\,(l) = \frac{J_{q,\mathrm{SW}}\,(l) + J_{q,\mathrm{NSW}}\,(l)}{q} \cdot M \cdot 1000 \tag{21}$$

$$\tilde{E}_q = \frac{E_O \cdot q}{M \cdot 1000} \tag{22}$$

Here $q = 5,\ 6,\ 7,\ 8$ is the charge state of the four O products, M=16, and $\mathrm{J_{Q,SW}}$ (l) and $\mathrm{J_{Q,NSW}}$ (l) are the SW and NSW O intensities for charge state q from the Lo L2 Species product.

Iron: Like O, we convert each of the individual charge state distributions to common units. Since the NSW Fe intensities are minimal compared to the SW Fe intensities and

Table 15 L3c Energy Ranges in [MeV/nuc]

Species	CoDICE-Lo	CoDICE-Hi
H	0.005 – 0.08	0.08 – 5.0
He	0.00025 – 0.04	0.04 – 5.0
O	0.0002 – 0.03	0.03 – 5.0
Fe	0.00009 – 0.015	0.02 – 5.0

they are not split into a high/low charge state product, we only use the SW Fe intensities assuming a charge state of $q_{\mathrm{Fe,low}} = 9$ and $q_{\mathrm{Fe,low}} = 15$ with a mass of M=56. The converted Fe intensities are given by:

$$\tilde{J}_{\mathrm{Fe,low}}(l) = \frac{\left(J_{\mathrm{low,SW}}(l)\right)}{q_{\mathrm{Fe,low}}} \cdot M \cdot 1000 \tag{23}$$

$$\tilde{J}_{\mathrm{Fe,high}}(l) = \frac{\left(J_{\mathrm{high,SW}}(l)\right)}{q_{\mathrm{Fe,high}}} \cdot M \cdot 1000 \tag{24}$$

$$\tilde{E}_{\mathrm{Fe,high}} = \frac{E_{\mathrm{Fe}} \cdot q_{\mathrm{Fe,high}}}{M \cdot 1000} \tag{25}$$

$$\tilde{E}_{\mathrm{Fe,low}} = \frac{E_{\mathrm{Fe}} \cdot q_{\mathrm{Fe,low}}}{M \cdot 1000} \tag{26}$$

Here, $J_{\mathrm{low,SW}}(l)$ and $J_{\mathrm{high,SW}}(l)$ are the SW low and high charge state Fe intensities from the Lo *L2 Species* product.

Step 2: CoDICE-Lo Energy Re-binning

We first define the energy-per-nuc range for each species to create the new set of energy-per-nuc bins. Each set will contain 20 logarithmic-spaced bins defined as follows:

1. Compute dE in log space by:

$$dE = \frac{\left(\log_{10}(E_{\max}) - \log_{10}(E_{\min})\right)}{20} \tag{27}$$

2. For $i = 0, \ldots, 19$ bins, the lower $E_{l,i}$, upper $E_{u,i}$, and center E_i in energy-per-nuc are:

$$E_{l,i} = 10^{\left(\log_{10}(E_{\min}) + i \cdot dE\right)} \tag{28}$$

$$E_{u,i} = 10^{\left(\log_{10}(E_{\mathrm{l,i}}) + dE\right)} \tag{29}$$

$$E_i = \sqrt{E_{u,i} \cdot E_{l,i}} \tag{30}$$

For CoDICE-Lo, the L3c energy ranges are determined from the minimum and maximum energies measured for each species assuming charge states of 1, 2, 6, and 10 for H, He, O, and Fe. For CoDICE-Hi, the minimum energy for each species is chosen to avoid overlap with the CoDICE-Lo energy ranges and the maximum energy is 5.0 MeV/nuc. These are listed in Table 15.

The re-binned intensities are computed by averaging the intensities produced in Step 1 over each of the newly defined energy-per-nuc ranges. For example:

$$\tilde{J}_{O,q}(i) = \frac{\left(\sum_{E_{l,i} \le \tilde{E}_O(l) < E_{u,i}} \tilde{J}_{O,q}(l)\right)}{N_i} \quad \text{for} \quad i = 0, 1, \ldots, 19 \quad \text{and} \quad q = 5, 6, 7, 8 \tag{31}$$

Here, N_i is the number of $\tilde{E}_O$ bin values that fall within the range $E_{l,i} - E_{u,i}$. This step results in a set of 20 intensities and energy-per-nuc bins for each species. For the O and Fe products, we sum the re-binned intensities over charge state.

$$\tilde{J}_O(i) = \sum_{q=5,6,7,8} \tilde{J}_{O,q}(i) \tag{32}$$

$$\tilde{J}_{\mathrm{Fe}}(i) = \tilde{J}_{\mathrm{Fe,low}}(i) + \tilde{J}_{\mathrm{Fe,high}}(i) \tag{33}$$

Step 3: Hi Intensities

The Hi L2 omni-directional intensities are provided as a function of energy-per-nuc bins at a cadence of 1-min. To avoid overlap between the Hi and Lo distributions, we restrict the energy-per-nuc range of the Hi data, as shown in Table 14. We then time-average the Hi intensity over each 4-min period corresponding to the Lo intensities in Step 2.

Step 4: Combine the Hi and Lo intensities

The Lo intensities from Step 2 are combined with the Hi intensities from Step 3 to form the final L3c product. The final data array provides intensities as a function of energy-per-nuc bins. The Lo and Hi intensities and energy-per-nuc arrays are concatenated to form single data and energy-per-nuc bin arrays. These are then provided as the *L3c Combined Energy Time Spectrograms*.

L3c Combined Pitch Angle Distributions are computed from the CoDICE-Hi L3b Pitch Angle Distributions and the CoDICE-Lo L2 Angular Intensities. CoDICE-Lo pitch angle distributions are first computed for He and O using the NSW and SW products and the magnetic field vector averaged over the Lo measurement time. The final L3c product contains combined He and O intensities from Hi and Lo as a function of pitch angle and energy at 4-min cadence.

7.5 I-ALiRT

I-ALiRT data products are created and formatted like the various counts products, but instead of being delivered to the S/C as single large packets, they are split into many small packets and transmitted over a ∼4-minute period. Table 16 lists the CoDICE I-ALiRT data products and their data volume in the S/C I-ALiRT telemetry stream (Lee et al. 2025).

CoDICE-Lo products consist of elemental abundances and charge state ratios of SW species from the SW sector. The ratios are computed by first converting I-ALiRT counts to intensities in the same way as the L2 Species Intensities, and then computing pseudo-densities of each species as follows:

$$psN_j = \sum_{l=0}^{128} \mathrm{J_j}(l) \cdot \sqrt{\left(\frac{E}{q}\right)_l} \cdot \sqrt{\left(\frac{M}{q}\right)_j} \tag{34}$$

Here, $\mathrm{J_j}(l)$ is the intensity for species j and energy-per-charge l. The final products are then ratios of psN_j for different species and charge states, given in Table 16.

Table 16 CoDICE I-ALiRT data products and volume (in bytes) per packet

	CoDICE-Lo: 15 bytes per packet	CoDICE-Hi: 5 bytes per packet
Products	*Elemental Abundance Ratios* for C/O, Mg/O, and Fe/O. Pseudo-densities are summed over all measured charge states at 4-min cadence. *Charge State Ratios* of C^{6+}/C^{5+}, O^{7+}/O^{6+}, and Fe^{low}/Fe^{high} at 4-min cadence.	*Proton Intensities* covering 0.05–5 MeV as a function of 4 spin and 4 polar angles at 1-min cadence.

CoDICE-Hi products consist of proton intensities in 15 energy bins as a function of four polar and four spin angles. The L1a proton counts are summed over every six spin sectors and in groups of three SSDs and then converted to intensities similarly to the L2 Omnidirectional Intensities.

8 Summary and Conclusions

The CoDICE instrument on board the IMAP mission is designed to simultaneously provide 1) the 3D velocity distribution functions and the elemental, isotopic, and ionic charge state composition of lower-energy solar wind, suprathermal, and interstellar pickup ions in CoDICE-Lo, and 2) the mass and isotopic composition and the arrival directions of higher-energy ions that are accelerated throughout the heliosphere in CoDICE-Hi. CoDICE also provides measurements of SW abundances and charge states, as well as the intensities of suprathermal protons in four different directions to the real-time I-ALiRT data stream for Space Weather research and monitoring.

CoDICE is an exceptionally capable, next generation instrument that combines the capabilities of two separate instruments in an innovative, compact design that includes 1) an electrostatic analyzer (ESA) and a common 2) Time-of-flight (TOF) vs. residual energy (E_{Res}) spectrometer. CoDICE-Lo uses a $6^\circ \times 360^\circ$ FOV ESA to select SW, PUIs, and suprathermal ions between ~0.5–80 keV/q according to their energy-per-charge (E/q), and together with coincident measurements of the same ion's TOF and E_{Res} in 24 APDs yields estimates of the ion's mass, charge state, and total incident energy. CoDICE-Hi uses 12 separate dual-foil $10^\circ \times 16^\circ$ collimators to measure the composition and arrival directions of the more energetic H-Fe ions between ~0.03–5 MeV/nuc. Coincident measurements of the same ion's TOF and E_{Res} in 12 SSDs yields estimates of the ion's mass and total incident energy. A key CoDICE innovation is that both CoDICE-Lo and CoDICE-Hi share the START and STOP MCPs and use the same TOF system for TOF measurement.

Detailed simulations and on-ground calibration campaigns have confirmed that CoDICE meets or exceeds all science and performance requirements for the IMAP mission. CoDICE L2 and L3 data products are well defined and required to 1) determine the LISM composition and flow properties and 2) discover the origin of the enigmatic ST tails and advance understanding of the acceleration of particles in the heliosphere. CoDICE also provides critical SW and suprathermal data to the I-ALiRT real-time Space Weather broadcast.

Acronym	**Definition**
3D VDFs	Three-dimensional velocity distribution functions
ABM	Absolute Beam Monitor
ACE	Advanced Composition Explorer
AEB	APD Energy Board
AGND	Analog Ground
APD	Avalanche Photodiode
APL	Applied Physics Laboratory
App	Application
ASIC	Application-Specific Integrated Circuit
Az	Azimuth
CDH	Command and Data Handling
CFD	Constant-Fraction Discriminator
CIR	Co-rotating Interaction Region
CME	Coronal Mass Ejection
CMOS	Complementary Metal-Oxide Semiconductor
CoDICE	Compact Dual Ion Composition Experiment
DAC	Digital-to-Analog Converter
DCR	Double coincidence rate
DSA	Diffusive shock acceleration
E/q	Energy-per-charge
Ebox	Electronics Box
E_{inc}	Incident Energy
ENA	Energetic neutral atom
E_{res}	Residual Energy
ESA	Electrostatic Analyzer
ESP	Energetic Storm Particle
FEE	Front-End-Electronics
FWHM	Full Width at Half Maximum
FIP	First Ionization Potential
FOV	Field-of-View
FPGA	Field-Programmable Gate Array
FSW	Flight software
GE	Energy Geometric Factor
GF	Geometric Factor
GLOWS	GLObal solar Wind Structure
GOES	Geostationary Operational Environmental Satellite
GSFC	Goddard Space Flight Center
HIT	High-energy Ion Telescope
HK	Housekeeping
HV	High Voltage
HVPS	High Voltage Power Supply
I&T	Integration and Testing
I/O	Input/Output
I-ALiRT	IMAP Active Link for Real-Time
ICD	Interface Control Document
ICE	IMAP Common Electronics
ICME	Interplanetary Coronal Mass Ejection
ID	Identifiers

IMAP	Interstellar Mapping and Acceleration Probe
IMF	Interplanetary Magnetic Field
IP	Interplanetary
IR&D	Internal Research & Development
L1	Level 1
LH	Left-hand
LISM	Local Interstellar Medium
LPI	Lines per Inch
LUT	Look-Up Table
LVPS	Low Voltage Power Supply
LZMA	Lempel-Ziv-Markov chain Algorithm
M	Mass
MAG	Magnetometer
MCP	Microchannel plate
MDM	Micro-D Metal
MiM	Metal-Insulator-Metal
MLI	Multi-Layer Insulation
MMS	Magnetospheric Multiscale Mission
MOSIS	Metal-Oxide Semiconductor Implementation Service
MRAM	Magnetoresistive Random Access Memory
MRD	Mission Requirements Document
NASA	National Aeronautics and Space Administration
NSO	No Scan Operation
NSW	Non-Sunward
PAB	Pre-Amplifier Board
PAC	Post-Acceleration
PCB	Printed Circuit Board
PEEK	Polyetheretherketone
PHA	Pulse-Height-Analysis
PROM	Programmable read only memory
PUI	Pickup Ion
q	Charge state
q/M (M/q)	Charge/Mass (Mass/Charge)
R	Rate
RC	Resistor Capacitor
RF	Radio Frequency
RGFO	Reduced Geometric Factor Operation
RH	Right-hand
RTS	Relative Times Sequence
S/C	Spacecraft
SCI_LUT	Science Lookup Table
SEB	SSD Energy Board
SEP	Solar Energetic Particle
SHV	Safe High Voltage
SIS	Solar Isotope Spectrometer
SP	STOP
SSD	Solid-State Detector
ST	START
STA	START-A

STB	START-B
STP-5	Solar Terrestrial Probe-5
SW	Solar Wind or Sunward Direction
SWAPI	Solar Wind and Pickup Ion
SWE	Solar Wind Electron
SWICS	Solar Wind Ion Composition Spectrometer
SwRI	Southwest Research Institute
TCR	Triple coincidence rate
TDC	Time to digital converter
TOF	Time-of-Flight
UV	Ultraviolet
VDF	Velocity Distribution Function

Acknowledgements We gratefully acknowledge the numerous contributions and collaborations from all the dedicated scientists, engineers, technicians, administrators, and other personnel who have made the CoDICE instrument and the IMAP mission a reality. We reserve special thanks for the IMAP project team at APL and the IMAP Leadership team for their full support and guidance during all phases of the CoDICE instrument and IMAP mission development. We acknowledge financial support from the Southwest Research Institute's Internal Research & Development Program (IR&D) which provided the resources needed for the initial concept study and the subsequent design and testing of the CoDICE prototype that eventually led to the successful selection for flight for the IMAP mission. We also acknowledge support from the IMAP project office at Goddard Space Flight Center (GSFC), and we especially thank Georgio de Nolfo, and Shri Kanekal for their leadership and help with interfacing with the GSFC IMAP mission assurance and management teams. This work is supported by the IMAP mission as a part of NASA's STP mission line (80GSFC19C0027). The authors have no conflicts of interest to declare that are relevant to the content of this article.

Declarations

Competing Interests The authors declare no competing interests.

References

Allegrini F, Ebert RW, Funsten HO (2016) Carbon foils for space plasma instrumentation. J Geophys Res Space Phys 121:3931. https://doi.org/10.1002/2016JA022570

Bzowski M, Wawrzaszek R, Strumik M, et al (2025) GLObal Solar Wind Structure (GLOWS). Space Sci Rev 221:105. https://doi.org/10.1007/s11214-025-01233-y

Christian ER, Mitchell JG, Albaijes D, et al (2026) The High-energy Ion Telescope (HIT) for the Interstellar Mapping and Acceleration Probe (IMAP) mission. Space Sci Rev 222

Cohen CMS, Alterman BL, Baker DN (2026) IMAP's role in understanding particle injection and energization throughout the heliosphere. Space Sci Rev 222. https://doi.org/10.1007/s11214-025-01257-4

Dahl DA (2000) SIMION for the personal computer in reflection. Int J Mass Spectrom Ion Process 200:3. https://doi.org/10.1016/S0168-1176(00)00329-0

Desai MI, Ogasawara K, Ebert RW, et al (2015) An integrated time-of-flight versus residual energy subsystem for a compact dual ion composition experiment for space plasmas. Rev Sci Instrum 86:5. https://doi.org/10.1063/1.4921706

Desai MI, Ogasawara K, Ebert RW, et al (2016) Compact Dual Ion Composition Experiment for space plasmas – CoDICE. J Geophys Res Space Phys 121:6632. https://doi.org/10.1002/2016JA022387
Desai MI, Ogasawara K, McComas DJ, et al (2017) Compact Dual Ion Composition Experiment. United States Patent No.: US 9,613,789 B1
Funsten HO, Harper RW, McComas DJ (2005) Absolute detection efficiency of space-based ion mass spectrometers and neutral atom imagers. Rev Sci Instrum 76:053301. https://doi.org/10.1063/1.1889465
Funsten HO, Allegrini FA, Reisenfeld DB, et al (2026) The Interstellar Mapping and Acceleration Probe High Energy (IMAP-Hi) Neutral Atom Imager. Space Sci Rev 222
Galvin AB (1982) Charge states of heavy ions in the energy range in the order of ∼30–130 keV/Q observed in upstream events associated with the Earth's bow shock. PhD thesis. University of Maryland
Horbury TS, O'Brien H, Greenaway C, et al (2026) The IMAP Magnetometer. Space Sci Rev 222
Hua Y, Chitnis D (2022) A highly linear and flexible FPGA-based time-to-digital converter. IEEE Trans Ind Electron 69:13744. https://doi.org/10.1109/TIE.2021.3128912
Lee CO, Christian ER, Sandoval L, et al (2025) Space weather science to enhance forecasting with the NASA IMAP Active Link for Real-Time (I-ALiRT) system. Space Sci Rev 221:117. https://doi.org/10.1007/s11214-025-01244-9
McComas DJ, Allegrini F, Baldonado J, et al (2009) The two wide-angle imaging neutral-atom spectrometers (TWINS) NASA mission-of-opportunity. Space Sci Rev 142:157. https://doi.org/10.1007/s11214-008-9467-4
McComas DJ, Christian ER, Schwadron NA, et al (2025) Interstellar Mapping and Acceleration Probe: the NASA IMAP Mission. Space Sci Rev 221:100. https://doi.org/10.1007/s11214-025-01224-z
Ogasawara K, Allegrini F, Desai MI, et al (2012) A linear mode avalanche photodiode for ion detection in the energy range 5–250 keV. IEEE Trans Nucl Sci 59:2601. https://doi.org/10.1109/TNS.2012.2210244
Ogasawara K, Livi SA, Allegrini F, et al (2016) Next-generation solid-state detectors for charged particle spectroscopy. J Geophys Res Space Phys 121:6075. https://doi.org/10.1002/2016JA022559
Rankin JS, McComas DJ, Alimaganbetov M, et al (2025) Solar Wind and Pickup Ion (SWAPI) instrument on NASA's Interstellar Mapping and Acceleration Probe (IMAP). Space Sci Rev 221:108. https://doi.org/10.1007/s11214-025-01229-8
Schwadron N, Shen M, Begley S, et al (2025) The IMAP-Lo instrument. Space Sci Rev 221:121 https://doi.org/10.1007/s11214-025-01234-x
Skoug RM, Schultz TB, Venhaus DM, et al (2026) The Solar Wind Electron (SWE) instrument for the Interstellar Mapping and Acceleration Probe Mission. Space Sci Rev 222
Szalay JR, Provornikova E, Ayari E, et al (2026) Direct samples of interstellar and interplanetary material with IMAP. Space Sci Rev 222

Authors and Affiliations

S.A. Livi[1,2] · M.I. Desai[1,2] · K. Ogasawara[1,2] · L. Kistler[3] · E. Möbius[3] · M.J. Starkey[1] · M.A. Dayeh[1,2] · D. Kataria[1] · H.A. Elliott[1,2] · S. Hart[1] · B. Alterman[4] · D.J. McComas[5] · C.J. Pollock[4] · J. Mukherjee[1] · J. Trevino[1] · S. Ferrell[1] · T. Brenner[1] · S.E. Pope[1] · M. Tapley[1] · K. Pavlas[1] · J.S. Rankin[5] · M.M. Shen[5] · L. Khoo[5] · M. Alimaganbetov[5] · J. Teifert[5] · E.M. Roemer[5] · M. Shaw-Lecerf[5] · J. Escobar[5] · E.R. Christian[4] · N.A. Schwadron[3,5] · M. Gkioulidou[6] · G. Grubbs[1] · M. Brysch[1] · M. Epperly[1] · D. George[1] · G. Dunn[1] · J. Ford[1] · C.L. Schwendeman[1] · M. Commons[7] · S. Persyn[1] · S. Jaskulek[6] · S. Weidner[5] · C. Bert[1] · M. Ferris[1] · B. Rodriguez[1] · C. Nunez[1] · C. Urdiales[1] · S. Cortinas[1] · H. Rodriguez[1]

✉ M.I. Desai
mdesai@swri.edu

1 Space Science & Engineering, Southwest Research Institute, San Antonio, USA

2 Department of Physics and Astronomy, University of Texas-San Antonio, San Antonio, USA

[3] Physics & Astronomy, University of New Hampshire, Durham, USA

[4] Heliophysics Division, NASA Goddard Space Flight Center, Greenbelt, USA

[5] Department of Astrophysical Sciences, Princeton University, Princeton, NJ, USA

[6] Space Exploration Sector, Johns Hopkins University Applied Physics Laboratory, Laurel, USA

[7] L-3 Communications, Vertex Aerospace, Universal City, USA